Research Square

Preprints are preliminary reports that have not undergone peer review.
They should not be considered conclusive, used to inform clinical practice,
or referenced by the media as validated information.

Volatile-mediated microbiome recruitment by Streptomyces albidoflavus G1 enhances suppression of apple ring rot pathogen Botryosphaeria dothidea

Shengzhi Guo
North West Agriculture and Forestry University
Arneeb Tariq
North West Agriculture and Forestry University
YaRong Luo
North West Agriculture and Forestry University
Xianyu Li
North West Agriculture and Forestry University
Zixu Wang
North West Agriculture and Forestry University
Zhinan Du
North West Agriculture and Forestry University
Qi Cheng
North West Agriculture and Forestry University
Jiangbo Qi
North West Agriculture and Forestry University
Junfeng Pan
North West Agriculture and Forestry University
Lingfang Zhu
North West Agriculture and Forestry University
Xihui Shen
xihuishen@nwsuaf.edu.cn

North West Agriculture and Forestry University

Research Article

Keywords:

Posted Date: June 1st, 2026

DOI: https://doi.org/10.21203/rs.3.rs-9610327/v1

License: This work is licensed under a Creative Commons Attribution 4.0 International License.
Read Full License

Additional Declarations: No competing interests reported.

Version of Record: A version of this preprint was published at Microbiome on October 13th, 2026. See the published version at https://doi.org/10.1186/s40168-026-02540-4.

Abstract

Background

Apple ring rot, caused by the fungal pathogen *Botryosphaeria dothidea*, is a devastating disease affecting apple production. It causes extensive damage to fruit and branches, leading to significant economic losses within the apple industry in China and across the globe. While the volatile organic compound G1-VOC has demonstrated remarkable efficacy in suppressing *B. dothidea* and reducing fruit decay, its internal biocontrol mechanism and the host transcriptional response remain largely unexplored.

Results

This study integrated microbiome analysis, VOC-bacterial interaction studies, and transcriptome profiling to investigate the mechanism by which G1-VOCs regulates apple endophytes to suppress apple ring rot. Initially, G1 was identified for its VOC-mediated biocontrol activity. GC-MS analysis showed compounds from sesquiterpenoid, triterpenoid, and phenylalanine metabolism pathways act as primary inhibitors, disrupting fungal glycolysis, membrane integrity, and biofilm formation. 16S rRNA analysis revealed G1-VOCs prevent bacterial diversity imbalances caused by *Staphylococcus* during infection while maintaining microbial stability by regulating *Pseudomonas* abundance and recruiting the antagonistic strain *Pseudomonas* sp. aNRL1. Interactions between G1-VOCs and aNRL1 suggested the volatiles modulate bacterial growth kinetics, biofilm formation and motility to favour antagonistic strain. Finally, transcriptome analysis demonstrated G1 treatment reactivates the Brassinosteroid signaling pathway and upregulates genes associated with the MAPK cascade, lipid metabolism, and cuticle/wax biosynthesis during pathogen challenge.

Conclusion

G1-VOCs regulate microbial composition in apple endophytic tissues by enriching antagonistic strain and reprogram the apple transcriptome by upregulating defence and signalling pathways to counteract *B. dothidea.*

1. Introduction

Apple (*Malus domestica* Borkh.) is one of the most widely cultivated fruit crops in temperate regions and holds substantial economic importance worldwide, with an annual production of nearly 97.88 million tonnes globally [1,2]. Apple ring rot (ARR), caused by *Botryosphaeria dothidea*, is a destructive disease that severely compromises fruit quality, leading to considerable postharvest losses during storage and transportation [3–5]. Currently, disease management relies predominantly on chemical fungicides such as pyrisoxazole and iprodione. However, their extensive and prolonged use has raised serious concerns, including pesticide residues, the emergence of resistant pathogen populations, and negative

environmental impacts [6–8]. Therefore, the development of sustainable and eco-friendly alternatives is urgently needed. Biological control has emerged as a promising strategy for managing postharvest diseases due to its safety and environmental compatibility [6,9,10]. Among the diverse biocontrol agents, *Streptomyces* species have attracted increasing attention because of their prolific capacity to produce a wide array of secondary metabolites with antimicrobial properties. Numerous studies have demonstrated that *Streptomyces* spp. can effectively suppress plant pathogens through mechanisms such as antibiotic production, competition, and emission of volatile organic compounds (VOCs). In particular, VOCs produced by *Streptomyces* exhibit strong inhibitory effects against fungal pathogens without requiring direct contact, making them especially suitable for postharvest disease control [3,11–13]. Collectively, these findings underscore the significant potential of *Streptomyces* species as effective biocontrol agents in both preharvest and postharvest systems.

Recent studies have highlighted the important role of microbial volatile organic compounds (VOCs) in mediating interspecies interactions and shaping microbial community assembly, thereby contributing to disease suppression [14–16]. Unlike diffusible metabolites, VOCs can act over long distances and influence both pathogens and surrounding microbiota without direct contact [16–18]. On fruit surfaces, where microbial communities are relatively simple yet highly dynamic, VOC-producing microorganisms can significantly alter the ecological balance by inhibiting pathogens and modulating the composition of beneficial taxa [19–21]. For example, VOCs emitted by *Streptomyces* spp. have been shown to suppress fungal pathogens [22,23] and mediate microbial interactions, thereby influencing community dynamics [24]. Such VOC-mediated interactions may lead to the establishment of protective microbial consortia that enhance host resistance and stability of the fruit microbiome [25,26]. In particular, *Streptomyces* species are prolific producers of diverse VOCs with strong antimicrobial activity, and their capacity to influence microbial community structure suggests a dual role in both direct pathogen inhibition and indirect microbiome recruitment [24,27]. These characteristics make VOC-producing *Streptomyces* promising candidates for microbiome-based strategies in postharvest disease management.

Our preliminary results demonstrated that *Streptomyces albidoflavus* G1 significantly inhibits the growth of *Botryosphaeria dothidea in vitro*. Notably, G1 exhibited a stronger inhibitory effect in vivo on apple fruit, suggesting the involvement of additional mechanisms beyond direct antagonism. This observation led us to hypothesize that G1 may influence or recruit other microorganisms that contribute to enhanced disease suppression. To test this, we analysed the impact of G1 on the composition and stability on the apple surface microbiome. We identified bacterial taxa uniquely enriched in G1-treated fruit, consistent with active recruitment. These G1-associated isolates displayed robust antagonistic activity against *B. dothidea* under both *in vitro* and *in vivo* assays, supporting their functional contribution to disease suppression. To uncover the basis of this cooperation, we quantitatively assessed interspecies interactions between G1 and the recruited strains. These analyses, including chemotactic attraction, swarming coordination, interaction intensity, and biofilm formation, revealed structured and potentially cooperative interactions. This study provides important insights into the microbiome-mediated

biocontrol mechanisms and offers the development of microbiome-based strategies for the postharvest management of ARR.

2. Materials and methods

2.1 Strains and culture conditions

Streptomyces albidoflavus G1 was isolated from the endophyte of asymptomatic 'Red Fuji' apple, whereas *Botryosphaeria dothidea* was isolated from apple fruits exhibiting ARR symptoms. The G1 strain was routinely cultured on ISP2 medium at 30°C for 48 h. For fermentation broth preparation, G1 was grown in liquid ISP2 medium, reaching maximum biomass at 72 h under shaking conditions at 30°C. G1 strain identification was performed by sequencing the whole-genome (Supplementary method S1) and *B. dothidea* was identified by molecular marker-based (ITS) sequencing. The whole-genome sequence of G1 and ITS sequence of *B. dothidea* were deposited to NCBI under the accession numbers JBWCIU000000000 and PZ212878 respectively. Primers for ITS sequencing are enlisted in table 1.

B. dothidea was cultured on potato dextrose agar (PDA) at 26°C for 7 days to promote conidiation. Conidial suspensions were prepared by flooding 15-days-old PDA plates with sterile distilled water, gently scraping the surface to release conidia, and filtering the resultant suspension through eight layers of sterile gauze. The conidial concentration was adjusted to 5×10^4 spores mL^{-1} using a hemocytometer [28]. For long-term storage, *B. dothidea* conidial suspension and G1 were preserved at -80°C in glycerol solution.

2.2 G1 potential to inhibit *B. dothieda in vitro* and host relevant conditions

The antifungal activity of G1 against *B. dothidea* was evaluated under *in vitro* and *in vivo* conditions following the protocol described in [29]. For *in vitro* assays, bipartite (BI) plates were used, where different volumes of 72 h-grown G1 culture suspension were inoculated on ISP2 agar medium in one compartment, and *B. dothidea* was inoculated on PDA in the opposite compartment. G1 was pre-incubated for 48 h prior to fungal inoculation, and radial growth of *B. dothidea* was measured when control mycelia reached the partition line. Colony area was calculated using the formula $A = a \times b \times \pi$, where *a* and *b* represent colony diameters measured along two perpendicular directions.

For *in vivo* assays, disease-free, uniformly sized 'Red Fuji' apples were purchased from a local market. Apples were surface-sterilized by rinsing with sterile distilled water, followed by immersion in 1% sodium hypochlorite for 2–3 min. Subsequently, apples were washed three times with sterile water, and air-dried under sterile conditions. At the equatorial region, a wound (approximately 3 mm depth) was created using a sterile pipette tip and inoculated with 50 µL of *B. dothidea* spore suspension (5×10^4 spores mL^{-1}). For G1-VOCs exposure, different volumes (200–1000 µL) of 72 h-grown G1 culture suspension

were spread onto ISP2 agar plates. Plates were incubated at 30°C for 48 h to allow G1 growth. The plates were then placed in sealed containers to maintain high humidity, together with the inoculated fruits positioned on sterile supports, ensuring no physical contact between G1 and apple. Each treatment consisted of six biological replicates. Containers were incubated at 28°C for 5 days, and disease progression was assessed by measuring lesion area (cm^2).

Fruit quality parameters were evaluated across different treatments following standardized procedures (Supplementary method S2).

2.3 G1-VOCs profiling and functional validation

VOC profiling was performed using headspace solid-phase microextraction (HS-SPME) coupled with GC–MS/MS (Agilent 8890–7000D). Briefly, samples were incubated under controlled conditions, and VOCs were adsorbed onto an SPME fibre exposed to the headspace. Metabolites were identified based on retention indices and comparison with spectral libraries, and semi-quantified using internal standards. Raw data were processed using MassHunter software, followed by filtering to remove coefficient of variation, CV > 0.5. Multivariate analyses, including principal component analysis (PCA) and orthogonal partial least squares-discriminant analysis (OPLS-DA), were performed in R. Differentially abundant volatiles (DAVs) were selected based on variable importance in projection (VIP > 1).

Selected DAVs were purchased and validated for antagonistic activity against *B. dothidea* through *in vitro* assays. Briefly, 10μL each individual VOCs were coated on PDA petriplates and *B. dothidea* disc was inoculated at the centre of the plate. Fungal growth was evaluated by measuring the colony diameters along two perpendicular axes, and the colony area (cm^2) was calculated.

2.4 Quantification of *B. dothidea* in apple lesion-margin tissues

Total DNA of *B. dothidea* was extracted using the Fungi Genomic DNA Extraction Kit from Solarbio. Absolute quantification of *B. dothidea* was performed using plasmid-based qPCR.

Briefly, a DNA fragment from *B. dothidea* genome was amplified using the primer pair BdEF1-F(GCCTTATCACTCTGGTGAGGGG) and BdEF1-R(TCGCATAGACGAACGTGAGTGG) [30]. Purified target gene fragments were cloned into the pMD19-T vector and transformed into *Escherichia coli*. Recombinant plasmids were extracted, quantified, and serially diluted to generate standard curves. Quantitative PCR was performed using a LightCycler® 96 system (Roche) with SYBR Green chemistry. Relative gene expression was calculated using the $2^{-}\Delta\Delta CT$ method [31].

2.5 Sample collection of apple lesion-margin tissues

A 72-hours grown bacterial culture suspension of G1 (1mL) or sterile water was inoculated on ISP2 petriplate and incubated at 30°C for 48 hours. Apple fruits were uniformly wounded (3 mm depth) along the equatorial region and inoculated with 50 μL *B. dothidea* spore suspension (5×10^4 spores mL^{-1}) or sterile water. Inoculated fruits were placed on sterile supports above the corresponding plates in sealed

containers to allow VOCs exposure without direct contact. Four treatments were established: BG (with *B. dothidea*, with G1), BM (with *B. dothidea*, without G1), WG (without *B. dothidea*, with G1), and WM (without *B. dothidea*, without G1). The 3mm deep rotten area from lesion-margin of apple was collected with a sterile scalpel after 120 h of incubation. Each sample consisted of six biological replicates. Samples were immediately frozen in liquid nitrogen and stored at − 80°C.

2.6 Nucleic acid extraction, 16S rRNA, ITS genes amplicon sequencing, and sequence processing

Total microbial DNA was extracted from the samples using the Bacterial Genome Extraction Kit (DP302-02, Tiangen), and DNA concentration was measured using a Qubit fluorometer (Invitrogen, USA). For bacterial amplification, the V4 region of the 16S rRNA gene was amplified using 515F (5'-GTGYCAGCMGCCGCGGTAA-3') and 806R (5'-GGACTACHVGGGTWTCTAAT-3') primers. PCR conditions included an initial denaturation at 98°C for 30 seconds, followed by 32 cycles of denaturation at 98°C for 10 seconds, annealing at 54°C for 30 seconds, and extension at 72°C for 45 seconds, with a final extension at 72°C for 10 minutes. PCR products were purified using AMPure XP Beads (Beckman Coulter, USA) and quantified using the Qubit fluorometer. Sequencing was performed on the NovaSeq 6000 sequencer (Illumina, USA), generating paired-end reads of 250 bp.

For fungal sequencing, DNA was extracted using the CTAB method, followed by quality assessment with agarose gel electrophoresis and quantification via a UV spectrophotometer. The ITS2 region of the fungal rRNA gene was amplified using ITS1F/ITS2 primers (5'-GTGARTCATCGAATCTTTG-3' and 5'-TCCTCCGCTTATTGATATGC-3'). PCR reactions were performed with Phusion Hot Start Flex 2X Master Mix in a 25 μL reaction system, with the same thermal cycling conditions as described for the bacterial amplicons. PCR products were purified and quantified, then sequenced as above.

2.7 Data pre-processing and Genus-level differential abundance

Raw 16S rDNA sequencing data were processed using standard workflows, including quality filtering, primer trimming, and chimera removal with DADA2 [32] (https://benjjneb.github.io/ dada2) and Vsearch. Sequences were clustered into ASVs and taxonomically assigned using the SILVA database [33] (https://www.arb-silva.de/) using Id taxa classifier, while the UNITE database was used for taxonomic classification of the fungal ASVs [34] (Table S3). Alpha diversity (Shannon index) was calculated using QIIME2 to assess microbial richness and composition. The bacterial genus level differential abundance analysis was performed using ANCOM-BC2 in R, and P-values were adjusted using the Holm method (Table S2). Taxa with q-values < 0.05 were considered significantly differential and visualized via heatmaps using log10-transformed relative abundance data.

2.8 Identification of Pathogen-Dependent ASVs

ASVs showing pathogen-dependent responses to G1-VOC were identified by intersecting those significantly enriched in BG relative to BM ($q < 0.05$) with those showing no significant change between WG and WM ($q \geq 0.05$ and $|log2FC| < 1$) (Table S7). ASVs enriched in BG relative to BM (BBEAs) and remaining stable between WG and WM (WWSAs) were considered pathogen-dependent responders.

2.9 Targeted comparison of *Pseudomonas* abundance

To further evaluate the treatment-associated behaviour of *Pseudomonas*, its relative abundance was compared in STAMP. For multiple-group comparisons, the Kruskal–Wallis H-test was used, followed by Tukey–Kramer post-hoc analysis with a 95% confidence level. For targeted two-group comparisons, Welch's two-sided t-test was applied, and confidence intervals were estimated using Welch's inverted method at the 95% confidence level. Multiple-testing correction was performed using the Benjamini–Hochberg false discovery rate (FDR) procedure. STAMP analysis was used as a supportive comparison and visualization of key taxa.

2.10 Absolute Quantification of *Pseudomonas* via qPCR

To quantify the absolute abundance of *Pseudomonas* on the apple surface, total genomic DNA was extracted by Bacteria genomic DNA extraction kit, Tiangen. The concentration and purity of the extracted DNA were assessed using a NanoDrop 1000 spectrophotometer (Thermo Fisher Scientific, USA). The absolute copy number of the *Pseudomonas* genus was determined by qPCR targeting the 16S rRNA gene with the *Pseudomonas*-specific primers Pse434F (5'-ACTTTAAGTTGGGAGGAAGGG-3') and Pse665R (5'-ACACAGGAAATTCCACCACCC-3') [35].

A standard curve was generated using ten-fold serial dilutions of a plasmid containing the target gene fragment, ranging from 10^{-2} to 10^{-8} copies/μL. The R^2 value of the standard curve was > 0.99, and the amplification efficiency was between 90% and 110%. Final results were expressed as picograms (pg) of *Pseudomonas* DNA per gram of apple tissue (pg DNA/g) based on the calculated weight of the peel samples.

2.11 Isolation of endophytic bacteria, ASV matching, and phylogenetic analysis

Bacterial isolation was conducted concurrently with the collection of apple lesion-margin tissues for sequencing after 120 hours of incubation. Simply, 2 g of apple lesion margin tissue were homogenized in pestle and mortar with 3 mL of sterile 0.85% NaCl, followed by shaking at 180 rpm for 30 min, and standing for 5 min at room temperature. Each suspension was centrifuged and diluted to obtain 10^{-1} bacterial suspensions. A 0.1 mL aliquot of each suspension was mixed with 0.9 mL of sterile 0.85% NaCl to prepare a 10^{-2} dilution of bacterial spores, which was serially diluted to 10^{-4}. A 0.1 mL aliquot of each of the 10^{-4}, 10^{-5}, and 10^{-6} dilutions was plated on LB and M9G (6.8 g Na_2HPO_4, 3.0 g KH_2PO_4, 0.5 g NaCl, 1.0 g NH_4Cl, 0.25 g $MgSO_4$·7H2O, 5.0 g glucose, and 0.1 g $CaCl_2$ per 1000mL of water) medium [36], with three replicates per gradient, and incubated upside down at 30℃ for 48–72 h. Distinct single

colonies exhibiting unique morphological and growth characteristics were selected and further purified on respective agar plates and preserved in sterilized glycerol later at − 80℃.

To associate differential ASVs with cultivable bacteria, PCR amplification of bacterial 16S rRNA sequencing was performed by universal 27F/1492R primers using Taq PCR Master Mix (Tiangen Biotech Co., Ltd., Beijing, China). The gene sequences were aligned against ASV sequences within the corresponding amplicon region using BLASTn. Isolates showing complete sequence identity across the amplicon region were considered matched to the respective ASVs.

To determine the phylogenetic position of the representative isolate aNRL1, 16S rRNA gene sequences of closely related type strains were downloaded from the List of Prokaryotic names with Standing in Nomenclature (LPSN). These reference sequences, together with the aNRL1 sequence, were used for phylogenetic tree construction.

2.12 aNRL1 potential to inhibit *B. dothieda in vitro* and host relevant conditions

The antifungal efficacy of the cell-free supernatant (CFS) from *Pseudomonas* sp. aNRL1 was evaluated *in vitro* against *B. dothidea*. The CFS was mixed with molten PDA at a 1:1 (v/v) ratio, while control plates received an equal volume of sterile LB medium. An actively growing mycelial plug (5 mm diameter) of *B. dothidea* was inoculated at the center of each plate. Following incubation at 26°C for 7 days, the antifungal activity was quantified by measuring the fungal colony area (cm^2).

To assess the biocontrol potential under host-relevant conditions, 100 µL of aNRL1 bacterial suspension (10^8 CFU/mL) was inoculated into 3 mm deep wounds on apple fruits. The apples were pre-incubated for 24 hours at 26°C to allow for aNRL1 colonization prior to *B. dothidea* challenge. The experiment comprised four treatment groups; BaM: *B. dothidea* without aNRL1 pretreatment, BaN: *B. dothidea* following aNRL1 pretreatment, WaM: Sterile water control (no *B. dothidea*, no aNRL1), WaN: aNRL1 treatment only (no *B. dothidea*).

The inoculated apples were incubated for six days, after which the lesion area (cm^2) was measured. Each treatment group consisted of six biological replicates, and the entire experiment was performed in triplicate to ensure reproducibility.

2.13 Effect of G1-VOCs on pathogenicity-related genes in *B. dothidea*

To evaluate the effects of G1-VOCs on the expression of pathogenesis-related genes, all selected VOCs were evenly spread onto the surface of PDA plates at a volume of 10 µL per VOC, with the exception of α-humulene, which was applied at 150 µL. Following VOCs application, *B. dothidea* was inoculated onto the prepared plates. Blank PDA plates without VOC treatment served as the control group. All cultures were incubated under identical conditions for 96 h, after which fungal biomass was harvested. RNA was extracted using the RNA Plant & Fungi Quick-Extraction Kit (Zhengzhou Kermie Biotechnology), followed

by cDNA synthesis using the EasyScript One-Step gDNA Removal and cDNA Synthesis SuperMix. Subsequently, gene expression analysis of *B. dothidea* virulence genes, including alcohol dehydrogenase (NADP+) (*Bdadh*), aldehyde dehydrogenase (NAD(P)+) (*Bdaldh3*), aldehyde dehydrogenase (NAD+) (*Bdaldh*), and aldose 1-epimerase (*Bdgalm*), was performed using qPCR with SYBR Green chemistry in a 10 μL reaction system. Relative gene expression levels were normalized using tubulin as the internal reference gene. Primer sequences used in this study are listed in Table S1.

2.14 Effect of G1-VOCs on membrane integrity of *B. dothidea*

Membrane integrity was assessed using 3μg mL^{-1} propidium iodide (PI) and 5 mg L^{-1} fluorescein diacetate (FDA) [37]. Actively growing mycelial plugs of *B. dothidea* were incubated on PDA with G1 suspension on both peripheries. For VOC treatments, 10 μL of VOCs were evenly coated onto PDA plates prior to the inoculation of *B. dothidea* disc, followed by incubation at 26°C for 7 days. After incubation, mycelia were collected and stained with PI and FDA for 30 mins. Excess dye was removed by washing with sterile buffer, and samples were observed under a fluorescence microscope. The proportion of FDA-positive cells was quantified as an indicator of metabolic activity, while PI-positive cells represented membrane-compromised cells.

All experiments were conducted with six biological replicates. For VOC assays, all plates were hermetically sealed to prevent gas exchange and ensure consistent exposure conditions.

2.15 *In vitro* quantification of VOC-mediated biofilm suppression via headspace exposure

To evaluate the impact of G1-VOCs on biofilm formation in *B. dothidea* and *Pseudomonas* sp. aNRL1, a modified microtiter plate assay was employed to ensure consistent headspace exposure. For aNRL1, a single colony was cultured in LB medium at 30°C to an OD_{600}=1.2, followed by seeding into fresh LB medium at a 1% inoculum ratio. Aliquots (200 μL) of the bacterial suspension were dispensed into individual wells of 96-well microtiter strips. For *B. dothidea*, a spore suspension (1×10^6 spores/mL) was diluted to 1×10^{-2} spores/mL in PDB medium; subsequently, 200 μL of this suspension was added to each well of a 24-well plate.

To facilitate volatile exposure without direct contact, the microtiter wells were placed inside sterile Petri dishes containing filter paper strips. Individual VOCs (10 μL) were applied directly to the filter paper, and the dishes were immediately sealed to create a saturated volatile environment. Filter paper strips impregnated with sterile water were placed in mock-treatment Petri plates. Following 72 hours of static incubation (30°C for aNRL1; 26°C for *B. dothidea*), the supernatant was gently aspirated using a 1-mL syringe. All wells were rinsed three times with PBS to remove non-adherent cells and air-dried. The established biofilms were stained with 2% crystal violet for 30 minutes subsequently rinsed three times with water to remove excess stain. Quantitative analysis was performed by solubilizing the stained biomass in 33% glacial acetic acid and measuring the absorbance at 590 nm.

2.16 Assessment of growth kinetics of aNRL1 under volatile exposure

To evaluate bacterial growth kinetics under VOC exposure, a single colony of strain aNRL1 was inoculated into LB medium and cultured at 30°C to an OD_{600}=1.2. This pre-culture was used to seed 3 mL of fresh LB medium at 1% inoculum ratio. To facilitate volatile exposure without direct contact, a filter paper disk impregnated with 10 µL of specific VOCs was secured inside the tube cap. Control treatments received filter paper disks impregnated with an equal volume of sterile water. The tubes were incubated at 30°C with continuous agitation, and OD_{600} values were recorded every 2 hours until the culture reached the stationary phase. All treatments were performed in triplicate to ensure reproducibility.

2.17 Swimming motility assay under volatile exposure

To evaluate the influence of G1-VOCs on bacterial chemotaxis and dispersal, swimming motility was assessed using King's B (KB) medium supplemented with 0.3% BD Bacto™ Agar. *Pseudomonas* sp. aNRL1 was cultured in LB medium at 30°C to OD_{600} = 1.2, followed by centrifugation and washing the pellet in M9 medium to remove residual nutrients. Aliquots (2 µL) of the standardized bacterial suspension were centrally spotted onto the KB swimming plates.

For volatile treatments, 10 µL of specific VOCs were applied to the interior surface of the Petri dish lids, while sterile water served as the mock control. The dishes were immediately sealed to facilitate headspace saturation. Following 12 hours of incubation at 30°C, the expansion of swimming halos was measured and photographed. The KB medium (1 L) was formulated with 10g tryptone, 1.232g $MgSO_4.7H_2O$, 15mL glycerol, and 1.963g $K_2HPO_4.3H_2O$. All experiments were conducted in triplicate to ensure statistical robustness.

2.18 RNA sequencing, transcriptomic analysis, and qRT-PCR validation

Apple lesion-margin tissues were collected for RNA sequencing in four groups with or without *B. dothidea* and G1. Total RNA was extracted using the E.Z.N.A.® Plant RNA Kit (Omega Bio-Tek, Darmstadt, Germany). Strand-specific RNA-seq libraries were constructed and sequenced on an Illumina NovaSeq™ 6000 platform by LC Bio Technology Co., Ltd. (Hangzhou, China).

Clean reads were aligned to the wheat reference genome using HISAT2 [38], and transcript assembly and expression quantification were performed with StringTie [39]. Differential gene expression analysis was conducted using DESeq2 [40], with false discovery rate (FDR) correction. Functional enrichment of differentially expressed genes (DEGs) was performed based on KEGG annotations. Gene set enrichment analysis (GSEA) was performed using ranked gene expression [41]. Normalized enrichment scores (NES) and statistical significance were calculated for each pathway, with pathways showing FDR < 0.05 considered significant.

Prior to qRT-PCR, 1 µg of total RNA from each sample was used for cDNA synthesis. Reverse transcription was performed using the EasyScript One-Step gDNA Removal and cDNA Synthesis SuperMix (TransGen Biotech, China) following the manufacturer's protocol. Some highly significant DEGs associated with stress responses were selected for transcriptional profiling. The housekeeping gene *tubulin* served as the endogenous reference for normalization across all reactions. Relative expression levels were calculated using the 2 − ΔΔCT method. All gene-specific primers are summarized in Table S1 (Supplementary Data).

2.19 Data analyses

Statistical analyses were performed using GraphPad Prism 9. Significant differences among more than two treatments were analyzed using one-way ANOVA and Duncan's multiple range test; differences between two treatments were analyzed using a t-test. All tests used significance set at $P < 0.05$. Graphs were created using GraphPad Prism 8.0.

3. Results

3.1 G1-mediated disease suppression and its potential role in microbiome regulation

To evaluate the involvement of microbiome-associated mechanisms in *B. dothidea* resistance, endophytic microbial communities within healthy apple tissues were explored. From this specific ecological niche, bacterial strain G1 was isolated and identified as possessing antagonistic activity against *B. dothidea*.

The potential of strain G1 to mitigate *B. dothidea*-induced apple ring rot (ARR) was subsequently assessed by comparing the *in vivo* efficacy of G1 cell suspensions against G1-derived VOCs. No significant difference was observed between the lesion areas of apples treated with G1-VOCs and those treated with G1-suspensions (Fig. 2A-2B). Notably, the antagonistic effects elicited by G1-VOCs alone were found to be comparable to those achieved via direct G1-suspension application.

The inhibitory impact of G1-VOCs was further investigated by applying varying volumes of G1-suspension to monitor *B. dothidea* mycelial growth *in vitro* and lesion progression *in vivo*. A significant, dose-dependent decrease in mycelial area was recorded as the volume of G1 suspension increased, reaching a minimum at 1000 µL. Statistical analysis confirmed distinct differences between treatments, with the largest mycelial areas consistently observed in mock controls. Similarly, apple lesion areas representing disease progression were significantly reduced in correlation with increased G1 suspension volumes. While the mock treatment showed the highest disease severity, the 1000 µL G1 treatment resulted the smallest recorded lesion area. These findings indicate high efficacy of G1-VOCs in suppressing fungal proliferation and mitigating disease advancement (Fig. 2C-2D).

Consistent with these observations, the BG (VOC-treated) group exhibited reduced lesion sizes relative to the BM (mock) group (Fig. 2E). Absolute quantification of *B. dothidea* within the fruit tissues was performed using a plasmid-based standard curve (Fig. S1), revealing a significantly lower pathogen load in the BG group compared to the BM group (4.35×10^{-5}), suggesting a profound reduction in pathogen colonization mediated by G1-VOCs despite the sustained presence of the pathogen in untreated samples (Fig. 2F).

3.2 Fruit Quality and Volatile Profiles of Apple Under G1-VOCs and *B. dothidea* Exposure

The influence of G1-VOCs and *B. dothidea* exposure on the physiological quality of apple fruit was systematically evaluated. In the BM (pathogen-only) treatment, fresh weight loss was significantly greater ($p = 5.8 \times 10^{-5}$) than in the BG group, suggesting a reduction in weight loss mediated by the G1 treatment in combination with *B. dothidea*. Notably, a slight weight gain was observed in the BG treatment group compared to the WM (mock) group ($p = 1.39 \times 10^{-4}$), likely attributable to enhanced moisture retention, whereas the mock group exhibited standard post-harvest weight loss (Fig. 2H).

Hardness was significantly higher in the WM group compared to the BM treatments ($p = 0.0088$), indicating a decrease in fruit texture stability induced by *B. dothidea*, while no significant difference was found in other treatments, suggesting G1-VOC-mediated protection of fruit structural integrity during *B. dothidea* infection (Fig. 2G).

The WM group exhibited the highest lightness values whereas the BM group displayed the lowest, indicating a reduction in apple lightness induced by *B. dothidea*. Lightness remained unaffected by G1 treatment, whether applied alone or in combination with the pathogen (Fig. S2A). Furthermore, no significant differences were observed across groups regarding red-green or yellow-blue coordinates (Fig. S2B-S2C).

Calculations of ΔE relative to the WM group showed significantly higher values in both the BG ($p = 0.009$) and BM ($p = 0.010$) groups compared with the WG group. These results suggest a distinct shift in color profiles induced by B. dothidea and G1 VOCs, whereas the WG group exhibited minimal color deviation from the mock (Fig. S2D). Texture-related properties, including chewiness, fracturability, and springiness, were statistically comparable across all treatment groups (Fig. S2E-S2G). However, titratable acidity (TA) differed significantly between the BG and BM groups ($p = 0.042$), with the BG group showing the highest TA. This elevation suggests a synergistic influence of *B. dothidea* and G1 on fruit acidity. Conversely, no significant differences in TA were observed between the WG and WM groups (Fig. S2H)., and soluble solid content (%) remained uniform across all treatments (Fig. S2I).

Electronic nose analysis was performed to characterize the VOC profiles emitted by apples across treatment groups. Among the sensor array, nitrogen oxides, S-organic, and S-chloroform sensors exhibited the most significant sensitivity to the treatments. The WM group displayed a distinct emission profile compared to the other groups, a finding validated by PCA. PCA results revealed clear separation

between treatment clusters, confirming significant shifts in volatile emission profiles dependent on the presence of G1 and *B. dothidea* (Fig. S2J).

Notably, the BG group clustered closely with the WG group, suggesting the dominance of G1-derived volatiles in shaping the overall aromatic landscape irrespective of pathogen presence. In contrast, the BM and WM groups remained distinct, highlighting the specific influence of *B. dothidea* and the absence of G1-VOCs on fruit volatile emissions (Fig. S2K).

3.3 Genomic characterization of G1 and volatilome GC–MS profiling

Whole-genome sequencing was conducted to determine the taxonomic identity of G1. Average nucleotide identity (ANI) analysis revealed a 98.98% similarity between G1 and *Streptomyces albidoflavus* NRRL-B-1271, supporting its classification within this species (Fig. 3A). This assignment was further validated by whole-genome-based phylogenetic analysis, placing G1 in a close cluster with *S. albidoflavus* NRRL-B-1271 and related *Streptomyces* species (Fig. S3).

Genome mining identified various biosynthetic gene clusters (BGCs), including NRPS, PKS, RiPPs, terpene, and siderophore clusters (Fig. 3B). The presence of terpene and other secondary metabolite clusters suggests a strong potential for bioactive volatile compounds production.

To characterize these metabolites, we performed GC-MS based VOCs profiling was performed on 72-hour G1 suspensions and blank ISP2 medium (CK) (Fig. 3C). Principal Component Analysis (PCA) demonstrated clear demarcation between the CK and G1 groups, reflecting the distinct metabolic signatures of strain G1 (Fig. 3D).

Consistent with the separation observed in the PCA, differential analysis of the volatilome based on variable importance in projection (VIP) scores and fold change thresholds identified a subset of significantly altered compounds between treatments (Fig. 3E). Of the detected metabolites, 103 compounds were upregulated and 153 were downregulated, while the majority (1290) showed no significant change. These findings suggested the distinct metabolic clustering of G1 arises from selective modifications to specific volatile compounds rather than a systemic reconfiguration of the entire volatilome.

To functionally interpret the metabolic shifts, identified VOCs were annotated using the KEGG database. Differential abundance (DA) analysis revealed significant enrichment of compounds associated with sesquiterpenoid and triterpenoid biosynthesis, as well as phenylalanine metabolism, in G1-treated samples (Fig. 3F). Additional pathways, including general secondary metabolite and terpene backbone biosynthesis, also exhibited positive trends, but with lower enrichment scores.

Reflecting the KEGG pathway enrichment findings, a heatmap of upregulated VOCs within selected metabolic routes revealed clear divergence between G1 and CK treatments (Fig. 3G). Compounds associated with sesquiterpenoid and triterpenoid biosynthesis (Class I), including humulene,

caryophyllene, and farnesol, as well as phenylalanine metabolism (Class II), such as cinnamic acid and phenylethyl alcohol, exhibited higher relative abundance in G1. These results demonstrated the selective enrichment of these pathways through the production of specific VOCs by strain G1.

To validate the antifungal potential of these enriched metabolites, selected compounds were evaluated against *B. dothidea* using *in vitro* mycelial growth inhibition assays (Fig. 3H). Caryophyllene, farnesol, phenylethyl alcohol, and cinnamic acid were incorporated into molten PDA (10 μL/plate), while humulene was applied at 100 μL/plate to compensate for its lower volatility. All tested compounds significantly suppressed mycelial growth relative to the control, evidenced by reduced colony areas and high statistical significance ($p < 0.01$).

Among the tested VOCs, phenylethyl alcohol and humulene exhibited the most potent inhibitory effects, resulting in near-complete suppression of fungal growth. Caryophyllene and farnesol also induced substantial inhibition, whereas cinnamic acid displayed a moderate but significant effect. These findings demonstrate varying degrees of antifungal potency of multiple VOCs enriched in the G1 treatment.

Collectively, these results provide functional evidence for the direct role of terpenoid biosynthesis and phenylalanine metabolism in inhibiting *B. dothidea*. This establishes a mechanistic link between G1-derived volatilome shifts and pathogen suppression.

3.4 G1 regulates core microbial communities to mitigate *B. dothidea* infection in apple fruits

To characterize the impact of G1-derived VOCs on the fruit-associated microbiota, we analyzed the microbial community structure at the lesion margin of apple tissues (Fig. 4A).

Bacterial alpha diversity, estimated by the Shannon index, was significantly lower in the BG group and highest in the WM group. This pattern suggests that the interaction between *B. dothidea* and the strain G1, selectively reshapes the marked reduction in bacterial diversity, whereas the absence of both treatments supports a more diverse bacterial community. Fungal alpha diversity showed a consistent trend: the more diverse community in the WM and WG group but significantly suppressed in all samples inoculated with *B. dothidea* (BG and BM), with or without G1 (BG and BM) (Fig. 4B).

At the phylum level, bacterial communities were predominantly by Proteobacteria and Actinobacteria (Fig. S4), consistent with the typical fruit-associated endosphere. However, genus level annotation revealed pronounced shifts across treatments (Fig. 4C). In the pathogen-free conditions (WM and WG), bacterial communities were relatively diverse, with genera such as *Bacillus, Acinetobacter, and Pantoea* contributing substantially to overall abundance. In contrast, the *B. dothidea* groups (BM and BG) showed markedly reconfigured community structure. Notably, *Pseudomonas* exhibited a dramatic increase in relative abundance in the BG treatment, accounting for > 90% of the total bacterial community, whereas it remained at low levels in WM and WG (< 5%) and was only moderately represented in BM.

In contrast, fungal communities exhibited a distinct pattern, with the mycobiota in both BM and BG groups becoming overwhelmingly dominated by *Botryosphaeria* (> 95%) following inoculation (Fig. 4C). The pronounced dominance of *Botryosphaeria* in the BM and BG treatments obscured any potential VOC-mediated differences within the fungal microbiome. Consequently, we shifted our focus to bacterial community, where sufficient diversity remained to detect VOC-mediated changes.

Heatmap analysis at genus-level further highlighted treatment-dependent bacterial shifts (Fig. 4D). Microbiome compositions of the WG and WM groups were significantly different from those of the BG and BM groups. The WG and WM groups exhibited a more even distribution of multiple genera, including *Acinetobacter, Anoxybacillus*, and *Clostridium*, reflecting a more balanced community in the absence of pathogen pressure. In BG and BM groups, while several genera displayed moderate fluctuations, *Pseudomonas* showed a distinct enrichment pattern specifically in BG samples, reinforcing its potential role as a key responder to G1-VOCs under pathogen pressure.

The maintenance of higher diversity in the WG group compared to the BG group indicates that G1-derived VOCs exert a targeted, rather than broad-spectrum, influence on the resident microbiota.

3.5 Targeted recruitment of *Pseudomonas* ASV_2 under *B. dothidea* infection

STAMP analysis confirmed *Pseudomonas* was significantly enriched in the BG group compared to both BM ($q = 1.82 \times 10^{-6}$) and WG ($q < 1.00 \times 10^{-15}$), whereas no significant difference was observed between WG and WM ($q = 0.529$) (Fig. 4E; Table S5). These results indicated that the *Pseudomonas* enrichment is not driven by VOC treatment alone, but is specifically associated with the combined presence of *B. dothidea* and G1-VOCs exposure.

Intersection of ASVs enriched under BG–BM (BBEAs) with those *B. dothidea*-free conditions WG–WM (WWSAs), and further overlapping with *Pseudomonas*-assigned ASVs (PAs), identified a single ASV (ASV_2), indicating a *Pseudomonas* species that specifically responded to the simultaneous presence of *B. dothidea* and G1-VOCs (Fig. 4G).

For rigorous validation of *Pseudomonas* abundance in amplicon analysis, absolute quantification by qPCR was performed. The standard curve exhibited high linearity and strong negative correlation between Ct values and log10 copies, indicating high reliability (Fig. S5). *Pseudomonas* quantification based on this assay, indicated four-fold ($p = 6.67 \times 10^{-7}$) greater *Pseudomonas* abundance in BG treatment as compared to BM (Fig. 4F) confirming the targeted recruitment of this genus.

3.6 Isolation and functional validation of VOC-recruited antagonist *Pseudomonas* sp. aNRL1

To evaluate the functional contribution of the enriched ASV_2 to *B. dothidea* resistance, endophytic bacteria were isolated from the lesion-margin tissues of BG-treated apples. A representative isolate, designated aNRL1, exhibited 100% sequence identity to ASV_2 (Table S8)). Phylogenetic analysis placed

aNRL1 within the *Pseudomonas* clade, showing 99.41% similarity to *Pseudomonas tolaaslii* ATCC 33618 (Fig. 4H; NCBI: PZ326826).

The antifungal efficacy of *Pseudomonas* sp. aNRL1 was confirmed *in vitro*, where the cell-free supernatant achieved 98.4% inhibition of *B. dothidea* mycelial growth (Fig. 4G). This potent antagonism translated to host-relevant conditions; inoculation with aNRL1 significantly reduced apple lesion areas by 78% compared to the control ($p = 1.05 \times 10^{-5}$; Fig. 5F). Collectively, these findings demonstrate G1-derived VOCs selectively recruit antagonistic *Pseudomonas* taxa during pathogen challenge, identifying *Pseudomonas* sp. aNRL1 as a key functional driver of microbiome-mediated disease suppression.

3.7 G1-VOCs suppress essential metabolic gene expression and membrane integrity in *B. dothidea*

To elucidate the mechanistic basis of growth inhibition, qRT-PCR was used to assess transcriptional changes in *B. dothidea* key metabolic genes (*adh*, *aldh*, *aldh3*, and *galm*) following VOC exposure (Fig. 5A). The *galm* gene was significantly downregulated by caryophyllene (0.49-fold), cinnamic acid (0.64-fold), and humulene (0.63-fold), whereas phenylethyl alcohol and farnesol showed no effect. Notably, all tested VOCs significantly suppressed *aldh3* expression, with cinnamic acid eliciting the most substantial reduction (0.32-fold).

Variable responses were observed for *aldh* and *adh* expression under different VOCs. Caryophyllene and farnesol significantly inhibited *aldh* expression (0.54-fold and 0.77-fold, respectively), while phenylethyl alcohol induced a 1.78-fold increase. Furthermore, *adh* expression was markedly attenuated by phenylethyl alcohol (0.25-fold), cinnamic acid (0.30-fold), humulene (0.56-fold), and caryophyllene (0.81-fold). These widespread transcriptional suppressions suggest G1-derived volatiles impair fungal virulence by targeting essential metabolic pathways (Fig. S6).

These transcriptional suppressions were accompanied by severe physical damage to the pathogen. Fluorescence microscopy using Propidium Iodide (PI) and Fluorescein Diacetate (FDA) staining revealed G1-VOCs significantly compromised *B. dothidea* membrane integrity (Fig. 5B). While mock-treated hyphae exhibited strong green fluorescence (FDA-positive), indicating active metabolism and intact membranes, VOC-treated mycelia showed intense red fluorescence (PI-positive). This shift confirms lethal membrane permeabilization across all VOC treatments, identifying cell membrane disruption as a primary mode of action for G1-mediated fungal inhibition.

3.8 G1-VOCs mediate the competitive interaction between *B. dothidea* and aNRL1

To evaluate the ecological impact of G1-VOCs on the interaction between the host-recruited *Pseudomonas* and the *B. dothidea*, growth kinetics, motility, and biofilm formation were assessed. Individual VOC treatments significantly inhibited the biofilm formation of *B. dothidea*, as evidenced by reduced optical density (OD=590nm) across all VOCs (Fig. 5E, left). Conversely, humulene and

caryophyllene significantly promoted the biofilm growth of *Pseudomonas* sp. aNRL1, while cinnamic acid and farnesol showed no inhibitory effect, and only phenylethyl alcohol resulted in suppression (Fig. 5E, right).

Time-course analysis of growth kinetics confirmed aNRL1 maintained robust growth under humulene, caryophyllene, and farnesol, frequently matching or exceeding mock-treated growth rates (OD=600nm). Conversely, cinnamic acid and phenyethylalcohol treatments induced a marked decrease in aNRL1 growth during later stationary phases (14 and 16 hours). These differential growth responses suggest the provision of a selective environment by specific G1-VOCs that favors the establishment of the aNRL1 (Fig. 5D).

Beyond growth, G1-derived volatiles significantly influenced the physiological traits associated with colonization. Swimming motility in *Pseudomonas* sp. aNRL1 was markedly enhanced by humulene, caryophyllene, and farnesol compared to the mock control (Fig. 5A). In contrast, cinnamic acid and phenylethyl alcohol significantly restricted bacterial movement. These data suggest a dual-action mechanism: specific G1-VOCs actively stimulate the dispersal and proliferation of the antagonistic *Pseudomonas* sp. aNRL1 while imposing strict growth limitations on the fungal pathogen *B. dothidea*.

3.9 G1-VOCs activated stress response signalling pathways under *B. dothidea* infection

The transcriptome of lesion margin tissues was analysed in four treatment groups same as designed for amplicon analysis (Fig. 5), in order to get a deeper understanding of the synergistic relation between the apple and G1 in response to *B. dothidea* stress. In this study, a total of 14406, 10777, 19444 and 1852 DEGs (treated/control fold change > 1, $q < 0.05$) were obtained for BG_BM group, BG_WG group, BM_WM and WG_WM group, respectively (Fig. 6A).

Gene Set Enrichment Analysis (GSEA) identified significantly differential biological pathways based on enrichment score. In the absence of the pathogen, G1-VOCs induced a defence primed state by significantly upregulating pathways associated with pathogen sensing and secondary metabolism. The highest enrichment scores occurred in sesquiterpenoid and triterpenoid biosynthesis and the MAPK signaling pathway. These results indicate G1-VOCs trigger early-stage defense signaling and the accumulation of specialized antimicrobial metabolites, preparing the healthy fruit for potential challenge.

Under *B. dothidea* stress, G1-VOC treatment shifted the apple's transcriptome to building physical barrier and lipid metabolism as prominent positive enrichment was scored in fatty acid elongation and cutin, suberine and wax biosynthesis. These results suggests that G1-VOCs mitigate fungal invasion by strengthening the cuticle and cell wall architecture. This shift from signaling (observed in WG) to structural fortification (observed in BG) and illustrates a dynamic, context-dependent resistance strategy (Fig. 6B).

Detailed analysis of the plant hormone signal transduction pathway revealed significant modulation of Brassinosteroid (BR) signaling, a key regulator of fruit growth and stress tolerance (Fig. 6C). In the comparison between *B. dothidea* infected groups (BG_BM), several core components of the BR pathway, including the receptor BRI1 and the signaling kinases BSK and BIN2, show strong upregulation ($log_2FC > 1.17$). This indicates G1-VOC treatment reactivates BR signaling during *B. dothidea* infection.

Conversely, in the BM_WM comparison, these same genes are heavily downregulated (log_2FC as low as -7.87), suggesting the pathogen normally suppresses BR signaling to weaken the fruit. By preventing this suppression, G1-VOCs help maintain cellular homeostasis and activate proteasomal degradation pathways necessary for defense. Collectivey, these results suggest BR signaling is not constitutive but rather dynamically upregulated by G1-VOCs specifically during *B. dothidea* challenge.

We performed qRT-PCR to determine the gene expression levels of 8 DEGs initially identified by RNA-Seq to validate our findings (Fig. 6D). The induced defense response genes, including acetyl-CoA carboxylase / biotin carboxylase 1 (ACACA) and 3-ketoacyl-CoA synthase (KCS), were significantly enriched after treatment with G1-VOCs during infection, with Log_2FC values of approximately 5.0 and 4.0, respectively. This upregulation suggests enhanced lipid biosynthesis which serves as a physical defense barrier against *B. dothidea*. Synergistic induction of acyl-[acyl-carrier protein] desaturase (FAB2) and long-chain-fatty-acid—CoA ligase (FadD), which reached Log_2FC levels near 5.0 and 8.0 in the BG group, results in the activation of lipid-related pathways to strengthen the structural integrity of the fruit cuticle.

Simultaneously, G1-VOC exposure triggered the robust overexpression of signaling and antioxidant genes, specifically mitogen-activated protein kinase kinase 3 (MKK3) and peroxidase (POD), with both showing Log_2FC increases above 6.0. This same upward trend occurred in ethylene and oxylipin biosynthetic genes, such as 1-aminocyclopropane-1-carboxylate synthase 1/2/6 (ACS1/2/6) and lipoxygenase (LOX2S), which increased significantly by Log_2FC factors of roughly 5.8 and 6.0 compared to untreated infected controls (BM). Therefore, G1-VOCs enhance the disease resistance of apple fruit, an effect attributed to synergistic regulation of biotic stress-related pathways and the overexpression of the MAPK signaling cascade. These results revealed G1-VOCs not only promoted the aforementioned gene expression but also had significant inhibitory effects on fungal colonization compared to the control group.

4. Discussion

Previous studies on apple ring rot by *Botryosphaeria dothidea* have primarily focused on chemical control strategies [42,43], the continuous use of which may leads to environmental concerns. Although current research on biocontrol approaches has made some progress, including some biocontrol strains and involvement of biosynthetic gene clusters like iturin fengycin [44–46]. However, the mechanisms by which biocontrol bacteria regulate fruit microbial communities to suppress diseases remain poorly understood. Specifically, the influence of the apple receptacle associated strains and the interactions among

pathogens, and other bacterial strains, remain largely unexplored. These issues represent critical gaps in current research on apple ring rot.

4.1 The importance of VOCs in mediating disease resistance in apple

In this study, we investigated the potential mechanisms by which endophytic biocontrol strain *Streptomyces albidoflavus* G1 isolated from asymptomatic 'Red Fuji' apples can enhance resistance to ARR caused by *B. dothidea.* By integrating volatilome profiling, systematic microbiome analysis, interaction between VOCs-endophytic bacteria and RNA sequencing, we uncover the mechanistic pathway of G1 antagonism. Our results demonstrated that the antifungal activity of G1 is primarily mediated by the secretion of bioactive VOCs, a specialized metabolic strategy consistent with established *Streptomyces*-mediated suppression of post-harvest pathogens [47–49]. *In vitro* analysis of G1-VOCs exhibited significant reduction in mycelium area of *B. dothidea*. Moreover, a dose-dependent inhibition of fungal expansion was observed with surface area reducing from 62 cm^2 to 12 cm^2 across a G1 suspension gradient of 200–1000 µL. This suppression was also effectively translated *in vivo*, where the apples subjected to the same concentration of VOCs by the same range of suspension gradient exhibited dose dependent attenuation. Beyond the visible reduction in lesion area on apple, a marked decrease in pathogen biomass was observed, as quantified by *B. dothidea* genomic copy numbers. This suggests that metabolic outputs of G1 disrupts the colonization ability of *B. dothidea.* The direct, dose-dependent relationship between *Streptomyces*-derived VOCs and *Aspergillus* has been previously established by Lyu *et al.*, [50]. Beyond this antifungal dose-dependent effect, Qin *et al*., [51] reported a similar correlation regarding plant growth promotion and the mitigation of salinity stress mediated by VOCs.

Previous studies confirmed that VOCs enhance fruit resistance to pathogens by increasing flavonoid content, callose deposition, antioxidant enzyme activities and upregulation of jasmonic acid salicylic acid pathways [52–54].

4.2 Terpenoid and Phenylalanine Metabolites Mediate Synergistic Disruption of Cellular Integrity and Glycolytic Inhibition

Volatilome profiling identified sesquiterpenoid and triterpenoid biosynthesis and phenylalanine metabolism as the two most significantly enriched KEGG pathways in strain G1. Secondary metabolites, related to terpenoids, are highly relevant for interactions between microorganisms and have been associated with the disease suppression [55]. Therefore, we also investigated the abundance patterns of metabolites related to terpenoids and phenylalanine metabolism [56]. Functional validation of the key metabolites within these pathways, Class I (humulene, caryophyllene, and farnesol) and Class II (cinnamic acid and phenylethyl alcohol), confirmed their potent antifungal activity, with all compounds significantly arresting the radial mycelial growth of *B. dothidea* in *in vitro* assays. This inhibition of *B.*

dothidea mycelial growth results from a combined breakdown of its cell membrane and core metabolic pathways, specifically glycolysis [57]. Microscopic observation of the fungal hyphae following VOC treatment and dual staining with PI/FDA confirmed irreversible physical damage to the *B. dothidea*. The appearance of red-stained hyphae indicates that PI successfully penetrated the compromised membranes and bound to the fungal DNA, which is a clear hallmark of cell death [58,59]. Simultaneously, our genetic analysis showed that all tested VOCs significantly reduced the expression of the *Bdadh, Bdaldh, and Bdaldh3* genes. These genes are pivotal for the interconversion of alcohols and the detoxification of aldehydes [60,61]. Their suppression suggests an accumulation of toxic metabolic intermediates and a disruption of the pyruvate bypass, a critical survival mechanism for fungi under environmental stress [62,63]. Furthermore, the downregulation of *Bdgalm* likely blocked the flow of carbohydrates into glycolysis, starving the fungus of the energy required for mycelial growth and cell wall repair [64]. Consequently, the potent biocontrol activity of strain G1 is driven by the synergistic inhibition of both cellular structure and metabolic function. By crippling these internal systems, the VOCs prevent *B. dothidea* from maintaining the physiological health required to infect the apple and expand disease lesions.

4.3 Volatile-mediated recruitment of *Pseudomonas* sp. aNRL1: Engineering a secondary biological barrier

Through systematic microbiome analysis, we investigated shifts in apple endophyte-associated community induced by G1-VOCs and *B. dothidea*. *Streptomyces* are prolific producers of alkaline volatiles capable of interkingdom interactions and VOC-mediated communication [24]. Our analysis revealed G1-VOCs potential to regulate the core microbial apple endophyte community (e.g., enriching *Pseudomonas* while suppressing *Pantoea*, *Staphylococcus*, and *Klebsiella*), maintaining microecological stability and preventing pathogen-induced diversity imbalances. This is consistent with the universal nature of pathogen induced disruption of microbial patterns observed in hosts like litchi; however, while [65] demonstrated microbiome restructuring by inoculation of *Bacillus* cells, our study highlights the specific efficacy of volatile-mediated recruitment.

Recent evidence validated the potential of plant-derived VOCs as independent initiators of cross-kingdom recruitment. These signals allow receiver plants to boost growth and biomass through the selective attraction of beneficial bacteria, such as the *Pseudomonas* and *Bacillus* recruitment observed in tomato roots exposed to potato-onion volatiles [16]. Similarly, pineapple root VOCs enhance the soil health of banana rhizosphere by recruiting the beneficial genera (*Bacillus, Pseudomonas* and *Aspergillus*) [66]. However, such examples remain scarce within the context of the fruit microbiome.

The significant enrichment of the *Pseudomonas* genus in BG-treated apples (Fig. 4D, F) highlights a targeted shift in the epiphytic community structure. Rather than a broad taxonomic change, G1-VOCs favoured a specific microbial recruitment strategy, increasing *Pseudomonas* DNA density nearly four-fold during *B. dothidea* challenge. This phenomenon supports the Calling from distance hypothesis, where

volatiles serve as long-range chemo-attractants to recruit beneficial microbes to a specific niche [67]. The isolation and validation of antifungal activity of *Pseudomonas* sp. aNRL1 supports the niche engineering as a secondary biological barrier. This interaction points to functional division of labor where G1 initiates defence through volatilome signalling and the recruited *Pseudomonas* sp. aNRL1 provides localized, high-potency antifungal suppression. Within this framework, the two taxa work synergistically and effectively in stabilizing the fruit's microecological homeostasis [68].

4.4 Stabilization of Post-harvest Quality Indices and Aromatic Profiles through Volatile-Mediated Suppression of *B. dothidea*

Beyond these molecular interactions, the efficacy of the G1 volatilome was further reflected in the preservation of key fruit quality indices, most notably in the stabilization of fruit biomass and hardness. The BM group exhibited the maximum weight loss and a significant decrease in fruit hardness compared to the mock control. This deterioration is likely due to *B. dothidea* secreting cell wall-degrading enzymes that compromise the cuticular wax layer and break down structural polysaccharides, leading to both rapid desiccation and tissue softening [69,70]. In contrast, the BG group showed minimal water loss than the BM group, indicating that the presence of strain G1 successfully preserved the structural integrity of the apple's natural water barrier and cell wall architecture [71]. Notably, the WG group not only prevented post-harvest weight loss but actually exhibited a weight increase compared to the mock-treated fruits, suggesting that G1 may enhance surface hydration through the production of hydrophilic biofilms and slower respiration rate [72]. Chemically, *B. dothidea* utilization of apple organic acids led to decrease TA values in BM relative to BG treatment. In addition, *B. dothidea* infection induces tissue browning and skin darkening, likely due to the oxidation of phenolic compounds following cellular collapse, resulting in a significant reduction in Lightness [73]. While the minimum ΔE in WG demonstrates that strain G1 preserves the apple’s aesthetic quality without altering skin pigmentation. Finally, E-nose analysis confirmed the mitigation of decay via shifts in the volatile profile; PCA results showed that BG and WG clustered closely and remained distinct from the BM treatment. The overlap in the radar chart suggests that G1 VOCs dominate the aromatic headspace, effectively masking the metabolic signatures of *B. dothidea* [74].Collectively, these physiological, chemical and aromatic shifts demonstrate that strain G1 provides a multi-layered protective effect by not only suppressing fungal proliferation but also neutralizing the metabolic impact of *B. dothidea*, thereby preserving the post-harvest shelf-life and sensory integrity of the fruit in a state nearly identical to healthy controls.

Declarations

Funding

This work was supported by the grant of the National Natural Science Foundation of China (32330004 to X.S., 32470039 and 32100149 to L.Z.), the Young Science and Technology Rising Star Project of Yangling

Demonstration Zone (Grant 2025KJXX-02 to L.Z.).

Acknowledgements

We thank Teaching and Research Core Facility at the College of Life Sciences (N. Fan, and X. Chen), State Key Laboratory for Crop Stress Resistance, and the Life Science Research Core Services (K. Huang) Northwest A&F University for technical support.

Author information

Shengzhi Guo, and Arneeb Tariq contributed equally to this work.

Correspondence to Lingfang Zhu, or Xihui Shen

Authors and Affiliations

Shengzhi Guo, Arneeb Tariq, Yarong Luo, Xianyu Li, Zixu Wang, Zhinan Du, Qi Cheng, Jiangbo Qi, Junfeng Pan, Lingfang Zhu, Xihui Shen

State Key Laboratory for Crop Stress Resistance and High-Efficiency Production, Shaanxi Key Laboratory of Agricultural and Environmental Microbiology, College of Life Sciences, Northwest A&F University, Yangling, Shaanxi, China

Authors' contributions

SG conceived the main research framework, designed and coordinated the study, performed the major apple fruit decay experiments, conducted microbiome and transcriptomic data integration, interpreted the multi-omics results, prepared the figures, and contributed to manuscript revision. AT performed bioinformatic analyses of microbiome and transcriptomic datasets and was the major contributor to manuscript writing. YL conducted VOC-mediated apple protection assays, pathogen inoculation experiments, and phenotypic evaluations. XL and ZW performed functional assays of selected VOCs, including fungal growth inhibition, bacterial growth, motility, and related phenotypic analyses. ZD and QC carried out qRT-PCR validation, pathogen quantification, and targeted microbial absolute quantification. JQ and JP contributed to GC–MS-based VOC profiling, compound identification, and methodology optimization. LZ provided experimental resources, supported project implementation, and revised the manuscript. XS conceived and supervised the project, secured funding, guided experimental design and data analysis, and critically revised the manuscript. All authors read and approved the final manuscript.

Ethics approval and consent to participate

Not applicable

Consent for publication

Not applicable

Competing interests

The authors declare that they have no competing interests

References

1. FAOSTAT 2024. FAOSTAT_data_en_3-29-2026. Published online 2024.
2. Gupta S, Saxena S. Endophytic Diaporthe citrichinensis as a new source to alleviate post-harvest fungal infections in apple (Malus x domestica Borkh.). *Int J Food Microbiol*. 2025;440(May). doi:10.1016/j.ijfoodmicro.2025.111289
3. Zhang Q, Yong D, Zhang Y, et al. Streptomyces rochei A-1 induces resistance and defense-related responses against Botryosphaeria dothidea in apple fruit during storage. *Postharvest Biol Technol*. 2016;115:30–37. doi:10.1016/j.postharvbio.2015.12.013
4. Xin L, Zhang R, Wang X, et al. Extracellular and intracellular infection of Botryosphaeria dothidea and resistance mechanism in apple cells. *Hortic Plant J*. 2023;9(2):209–223. doi:https://doi.org/10.1016/j.hpj.2022.05.001
5. Wang X, Kong X, Qiu L, et al. MdWRKY45 contributes to resistance against Botryosphaeria dothidea in apple. *Postharvest Biol Technol*. 2024;213:112866. doi:https://doi.org/10.1016/j.postharvbio.2024.112866
6. Patiyal A, Pandit D, Mushtaq M. A systematic review of recent developments and trends in fungicide residue analysis in agriculture crops. *Microchem J*. 2026;220:116502. doi:https://doi.org/10.1016/j.microc.2025.116502
7. Tang FHM, Wyckhuys KAG, Li Z, Maggi F, Silva V. Transboundary impacts of pesticide use in food production. *Nat Rev Earth Environ*. 2025;6(6):383–400. doi:10.1038/s43017-025-00673-y
8. Zhang B, Yang Z, Wang C, Sun Y, Zhao Y, Huang Q. Fungicide-enhanced differentiation and multidrug resistance of Botrytis cinerea on greenhouse tomato. *Pestic Biochem Physiol*. 2025;215:106707. doi:https://doi.org/10.1016/j.pestbp.2025.106707
9. Zhou Q, Zhou Y, Wang L, et al. Harnessing beneficial microbes to boost sprout and microgreen production: current knowledge and future perspectives. *Crit Rev Food Sci Nutr*. 2026;66(2):259–277. doi:10.1080/10408398.2025.2522366
10. He J, Liu Z, Li G, et al. Innovative strategies: using nontraditional chemical methods to enhance the application of biocontrol agents in post-harvest preservation of agricultural products. *Crit Rev Food*

Sci Nutr. 2026;66(2):409–427. doi:10.1080/10408398.2025.2525448

11. Fan H, Zhang R, Lu J, et al. Streptomyces sp. 30702 composite chitosan alleviates continuous cropping obstacles in Chinese yam by improving rhizospheric soil microbial environment: A field study in Hainan. *Environ Technol Innov*. 2025;37:103936. doi:https://doi.org/10.1016/j.eti.2024.103936
12. Kim DR, Jeon CW, Cho G, et al. Glutamic acid reshapes the plant microbiota to protect plants against pathogens. *Microbiome*. 2021;9(1):1–18. doi:10.1186/s40168-021-01186-8
13. Hu L, Jia R, Sun Y, et al. Streptomyces pratensis S10 Controls Fusarium Head Blight by Suppressing Different Stages of the Life Cycle and ATP Production. *Plant Dis*. 2023;107(5):1442–1451. doi:10.1094/PDIS-09-22-2063-RE
14. Weisskopf L, Schulz S, Garbeva P. Microbial volatile organic compounds in intra-kingdom and inter-kingdom interactions. *Nat Rev Microbiol*. 2021;19(6):391–404. doi:10.1038/s41579-020-00508-1
15. Grandi L, Ye W, Clancy M V., et al. Plant-to-plant defence induction in cotton is mediated by delayed release of volatiles upon herbivory. *New Phytol*. Published online December 1, 2024. doi:10.1111/nph.20202
16. Zhou X, Zhang J, Shi J, et al. Volatile-mediated interspecific plant interaction promotes root colonization by beneficial bacteria via induced shifts in root exudation. *Microbiome*. 2024;12(1):207. doi:10.1186/s40168-024-01914-w
17. Farag MA, Song GC, Park Y soon, et al. Biological and chemical strategies for exploring inter- and intra-kingdom communication mediated via bacterial volatile signals. 2017;12(7):1359–1377. doi:10.1038/nprot.2017.023
18. Gupta DR, Paul SK, Ino M, Oowatari Y, Ueno M. Bacillus safensis NI2B displays strong antagonistic activities against rice blast pathogen Pyricularia oryzae through the production of volatile compounds. *Phytopathol Res*. 2025;7(1). doi:10.1186/s42483-025-00340-6
19. Olimi E, Kusstatscher P, Wicaksono WA, Abdelfattah A, Cernava T, Berg G. Insights into the microbiome assembly during different growth stages and storage of strawberry plants. *Environ Microbiome*. 2022;17(1):21. doi:10.1186/s40793-022-00415-3
20. Wassermann B, Abdelfattah A, Müller H, Korsten L, Berg G. The microbiome and resistome of apple fruits alter in the post-harvest period. *Environ Microbiome*. 2022;17(1):10. doi:10.1186/s40793-022-00402-8
21. Giese M, Stefani E, Larger S, et al. The blueberry phyllosphere microbiota: tissue-specific core communities and their stability across cultivars and years. *BMC Plant Biol*. 2025;25(1):947. doi:10.1186/s12870-025-06871-6
22. Cuervo L, Álvarez-García S, Salas JA, Méndez C, Olano C, Malmierca MG. The Volatile Organic Compounds of Streptomyces spp.: An In-Depth Analysis of Their Antifungal Properties. *Microorganisms*. 2023;11(7):1820. doi:10.3390/microorganisms11071820
23. Cordovez V, Carrion VJ, Etalo DW, et al. Diversity and functions of volatile organic compounds produced by Streptomyces from a disease-suppressive soil. *Front Microbiol*. 2015;Volume 6-.

https://www.frontiersin.org/journals/microbiology/articles/10.3389/fmicb.2015.01081

24. Jones SE, Elliot MA. Streptomyces Exploration: Competition, Volatile Communication and New Bacterial Behaviours. *Trends Microbiol*. 2017;25(7):522–531. doi:10.1016/j.tim.2017.02.001
25. Schmidt R, Cordovez V, De Boer W, Raaijmakers J, Garbeva P. Volatile affairs in microbial interactions. *ISME J*. 2015;9(11):2329–2335.
26. Berg G, Rybakova D, Grube M, Köberl M. The plant microbiome explored: implications for experimental botany. *J Exp Bot*. 2016;67(4):995–1002. doi:10.1093/jxb/erv466
27. Poveda J. Beneficial effects of microbial volatile organic compounds (MVOCs) in plants. *Appl Soil Ecol*. 2021;168:104118. doi:https://doi.org/10.1016/j.apsoil.2021.104118
28. Bellino M, Waite-Cusic J, Wang Q. Multi-method in vitro assessment of ultraviolet-C treatment against conidia and hyphal fragments of Botrytis cinerea. *Appl Environ Microbiol*. 2025;91(12). doi:10.1128/aem.01413-25
29. Black C, Disease S, Gong Y, et al. Antifungal Volatile Organic Compounds from *Streptomyces*. 2022;88(6):1–17.
30. Kwon G, Kim KH. Design and Validation of Specific qPCR Primers for Soil-Borne and Apple Tree-Associated Phytopathogenic Fungi. *Plant Pathol J*. 2025;41(4):532.
31. Livak KJ, Schmittgen TD. Analysis of relative gene expression data using real-time quantitative PCR and the 2 – ΔΔCT method. *methods*. 2001;25(4):402–408.
32. Rosen MJ, Callahan BJ, Fisher DS, Holmes SP. Denoising PCR-amplified metagenome data. *BMC Bioinformatics*. 2012;13(1):283. doi:10.1186/1471-2105-13-283
33. No Title. 10.1093/nar/gks1219
34. Abarenkov K, Nilsson RH, Larsson KH, et al. The UNITE database for molecular identification and taxonomic communication of fungi and other eukaryotes: sequences, taxa and classifications reconsidered. *Nucleic Acids Res*. 2024;52(D1):D791-D797. doi:10.1093/nar/gkad1039
35. Pereira RPA, Peplies J, Mushi D, Brettar I, Höfle MG. Pseudomonas-Specific NGS Assay Provides Insight Into Abundance and Dynamics of Pseudomonas Species Including P. aeruginosa in a Cooling Tower. *Front Microbiol*. 2018;Volume 9–2018. https://www.frontiersin.org/journals/microbiology/articles/10.3389/fmicb.2018.01958
36. Azatian SB, Kaur N, Latham MP. Increasing the buffering capacity of minimal media leads to higher protein yield. *J Biomol NMR*. 2019;73(1):11–17. doi:10.1007/s10858-018-00222-4
37. Huang X, Liu W, Dong F, Xu Y, Tian S, Chen T. Sapindus mukorossi saponins inhibit gray mold on strawberry fruit by impairing membrane integrity and organellar homeostasis of Botrytis cinerea. *Postharvest Biol Technol*. 2024;207:112594. doi:https://doi.org/10.1016/j.postharvbio.2023.112594
38. Kim D, Paggi JM, Park C, Bennett C, Salzberg SL. Graph-based genome alignment and genotyping with HISAT2 and HISAT-genotype. *Nat Biotechnol*. 2019;37(8):907–915. doi:10.1038/s41587-019-0201-4

39. Pertea M, Pertea GM, Antonescu CM, Chang TC, Mendell JT, Salzberg SL. StringTie enables improved reconstruction of a transcriptome from RNA-seq reads. *Nat Biotechnol*. 2015;33(3):290–295. doi:10.1038/nbt.3122
40. Love MI, Huber W, Anders S. Moderated estimation of fold change and dispersion for RNA-seq data with DESeq2. *Genome Biol*. 2014;15(12):550. doi:10.1186/s13059-014-0550-8
41. Subramanian A, Tamayo P, Mootha VK, et al. Gene set enrichment analysis: A knowledge-based approach for interpreting genome-wide expression profiles. *Proc Natl Acad Sci*. 2005;102(43):15545–15550. doi:10.1073/pnas.0506580102
42. Du HF, Zhang YH, Li W, et al. Antifungal Activity and Mechanism of Diaporthein B against Botryosphaeria dothidea in Prevention of Apple Ring Rot. *J Agric Food Chem*. 2024;72(38):20892–20904. doi:10.1021/acs.jafc.4c06101
43. Sosa MC, Lutz MC, Lódolo X, Basso CN. In vitro and in vivo activity of chemical fungicides and a biofungicide for the control of wood diseases caused by botryosphaeriales fungi in apple and pear. *Int J Pest Manag*. 2022;68(4):328–338. doi:10.1080/09670874.2022.2116660
44. fusarium mutant.pdf.
45. Chen X, Zhang Y, Fu X, Li Y, Wang Q. Isolation and characterization of Bacillus amyloliquefaciens PG12 for the biological control of apple ring rot. *Postharvest Biol Technol*. 2016;115:113–121. doi:https://doi.org/10.1016/j.postharvbio.2015.12.021
46. Mu Y, Yue Y, Gu G, Deng Y, Jin H, Tao K. Identification and characterization of the Bacillus atrophaeus strain J-1 as biological agent of apple ring rot disease. *J Plant Dis Prot*. 2020;127(3):367–378. doi:10.1007/s41348-020-00309-x
47. Li W, Ma J, Long Y, et al. Antifungal mechanisms of volatile organic compounds from Streptomyces albidoflavus SC-3 against postharvest kiwifruit rot caused by Botryosphaeria dothidea. *Food Microbiol*. 2026;137:105053.
48. Zhong J, Bai XY, Zhang Z, Li XG, Zhu JZ. Biocontrol potential of Streptomyces lactacystinicus producing volatile organic compounds against postharvest anthracnose of chili pepper. *Postharvest Biol Technol*. 2025;230:113758.
49. Li X, Zhang L, Zhao Y, et al. Biocontrol potential of volatile organic compounds produced by Streptomyces corchorusii CG-G2 to strawberry anthracnose caused by Colletotrichum gloeosporioides. *Food Chem*. 2024;437:137938.
50. Lyu A, Yang L, Wu M, Zhang J, Li G. High efficacy of the volatile organic compounds of Streptomyces yanglinensis 3–10 in suppression of Aspergillus contamination on peanut kernels. *Front Microbiol*. 2020;11:142.
51. Qin YY, Gong Y, Kong SY, et al. Aerial signaling by plant-associated Streptomyces setonii WY228 regulates plant growth and enhances salt stress tolerance. *Microbiol Res*. 2024;286(May):127823. doi:10.1016/j.micres.2024.127823
52. Li Z, Liu Q, Wu C, et al. Metschnikowia Pulcherrima yeast T-2 VOCs enhances postharvest blueberry fruit resistance to Botrytis cinerea by activating flavonoid metabolic pathways. *LWT*.

2024;201:116112. doi:https://doi.org/10.1016/j.lwt.2024.116112

53. Han FL, Zhao JX, Wang MY, et al. Multifaceted biocontrol mechanisms of Bacillus amyloliquefaciens F028 against Botrytis cinerea in postharvest tomato fruit. *Int J Food Microbiol*. 2026;455:111766. doi:https://doi.org/10.1016/j.ijfoodmicro.2026.111766
54. Sun L, Gao J, Tan Y, et al. Biocontrol of Apple Valsa Canker by Bacillus sp. H12 and modulation of the apple seedlings microbiome. *Pestic Biochem Physiol*. 2026;218:106946. doi:https://doi.org/10.1016/j.pestbp.2026.106946
55. Wei Z, Li C, Song F, et al. A farnesol-sensing triad in Pseudomonas aeruginosa drives interkingdom predation on Candida albicans via signal transduction. *Proc Natl Acad Sci*. 2026;123(17):e2529531123. doi:10.1073/pnas.2529531123
56. Pang L, Wu Y, Pan Y, Ban Z, Li L, Li X. Insights into exogenous melatonin associated with phenylalanine metabolism in postharvest strawberry. *Postharvest Biol Technol*. 2020;168:111244. doi:https://doi.org/10.1016/j.postharvbio.2020.111244
57. Huang Y, Li J, Shan X, Wang H, Duan Y. Bioactivities evaluation of an endophytic bacterial strain Bacillus tequilensis QNF2 inhibiting apple ring rot caused by Botryosphaeria dothidea on postharvest apple fruits. *Food Microbiol*. 2024;123:104590. doi:https://doi.org/10.1016/j.fm.2024.104590
58. Wang X, Chang L, Lian Q, et al. Antifungal Activity of Surfactin Against Cytospora chrysosperma. *Biomolecules*. 2025;16(1):51.
59. Fan L, Wei Y, Chen Y, et al. Epinecidin-1, a marine antifungal peptide, inhibits Botrytis cinerea and delays gray mold in postharvest peaches. *Food Chem*. 2023;403:134419. doi:https://doi.org/10.1016/j.foodchem.2022.134419
60. Gutiérrez-Corona JF, González-Hernández GA, Padilla-Guerrero IE, et al. Fungal alcohol dehydrogenases: Physiological function, molecular properties, regulation of their production, and biotechnological potential. *Cells*. 2023;12(18):2239.
61. Zhou J, Lin Y, Fu Y, Xie J, Jiang D, Cheng J. A cinnamyl alcohol dehydrogenase required for sclerotial development in Sclerotinia sclerotiorum. *Phytopathol Res*. 2020;2(1):13.
62. Fan J, Huang X, Zheng G, et al. Knockout of the aldehyde dehydrogenase gene in Fusarium oxysporum for enhanced ethanol yield. *Energies*. 2022;16(1):427.
63. Yan S, Ma JJ, Wu D, Huang GL, Yu XW, Wang YN. Value-added biotransformation of agricultural byproducts by cellulolytic fungi: a review. *Crit Rev Biotechnol*. 2025;45(4):982–1001.
64. Xu Y, Zhang Y, Zhu J, et al. Phytophthora sojae apoplastic effector AEP1 mediates sugar uptake by mutarotation of extracellular aldose and is recognized as a MAMP. *Plant Physiol*. 2021;187(1):321–335.
65. Zheng L, Lv X, Fu A, et al. Bacillus amyloliquefaciens PP19 regulation of microbial communities and suppression of Peronophythora litchii. *Microbiome*. Published online 2025. doi:10.1186/s40168-025-02239-y

66. Chen X, Lu Y, Jiang T, et al. Three Pineapple Root VOCs Affect Soil Health via Microbial Changes in Banana Rhizosphere. *Agronomy*. 2025;15(11):2520. doi:10.3390/agronomy15112520
67. Saskia KS bohm, Maria G, Jasper H, Wietse M, Garbeva P. Calling from distance: attraction of soil bacteria by plant root volatiles. *ISME J*. Published online 2018:1252–1262. doi:10.1038/s41396-017-0035-3
68. West SA, Cooper GA. Division of labour in microorganisms: an evolutionary perspective. *Nat Publ Gr*. doi:10.1038/nrmicro.2016.111
69. Wang Z, Wu M, Liao Q, Wang Y, Sui Y, Gong C. Current status and future trends of eco-friendly management of postharvest fungal decays in tomato fruit. *npj Sci Food*. 2025;9(1):104. doi:10.1038/s41538-025-00477-w
70. Lee GH, Min CW, Wang Y, Gupta R, Kim ST. Understanding the functional role of cell wall-degrading enzymes in Magnaporthe oryzae and their interactions with the rice immune system. *Plant Physiol Biochem*. 2026;231:111027. doi:https://doi.org/10.1016/j.plaphy.2026.111027
71. Sui Y, Li Z, Xiao X, Deng W, Duan B. The role of induced resistance in mitigating postharvest fungal diseases in fruits and vegetables. *J Adv Res*. 2026;83:91–111. doi:https://doi.org/10.1016/j.jare.2025.08.037
72. Chen J, Wei X, Lu X, et al. Burkholderia cenocepacia ETR-B22 volatile organic compounds suppress postharvest grey mould infection and maintain aroma quality of tomato fruit. *LWT*. 2022;165:113715. doi:https://doi.org/10.1016/j.lwt.2022.113715
73. Chen X, Xu C, Duan R, Haran Y, Li J, Yan S. Synergistic Oxalate-Phosphate Complex Inhibits Blue Stain and Preserves Freshness of Postharvest Lotus Rhizomes. *LWT*. Published online 2025:118397.
74. Yan H, Chen H, Zhao J, Yao T, Ding X. Postharvest H2O2 treatment affects flavor quality, texture quality and ROS metabolism of 'Hongshi' kiwifruit fruit kept at ambient conditions. *Food Chem*. 2023;405:134908. doi:https://doi.org/10.1016/j.foodchem.2022.134908

Figures

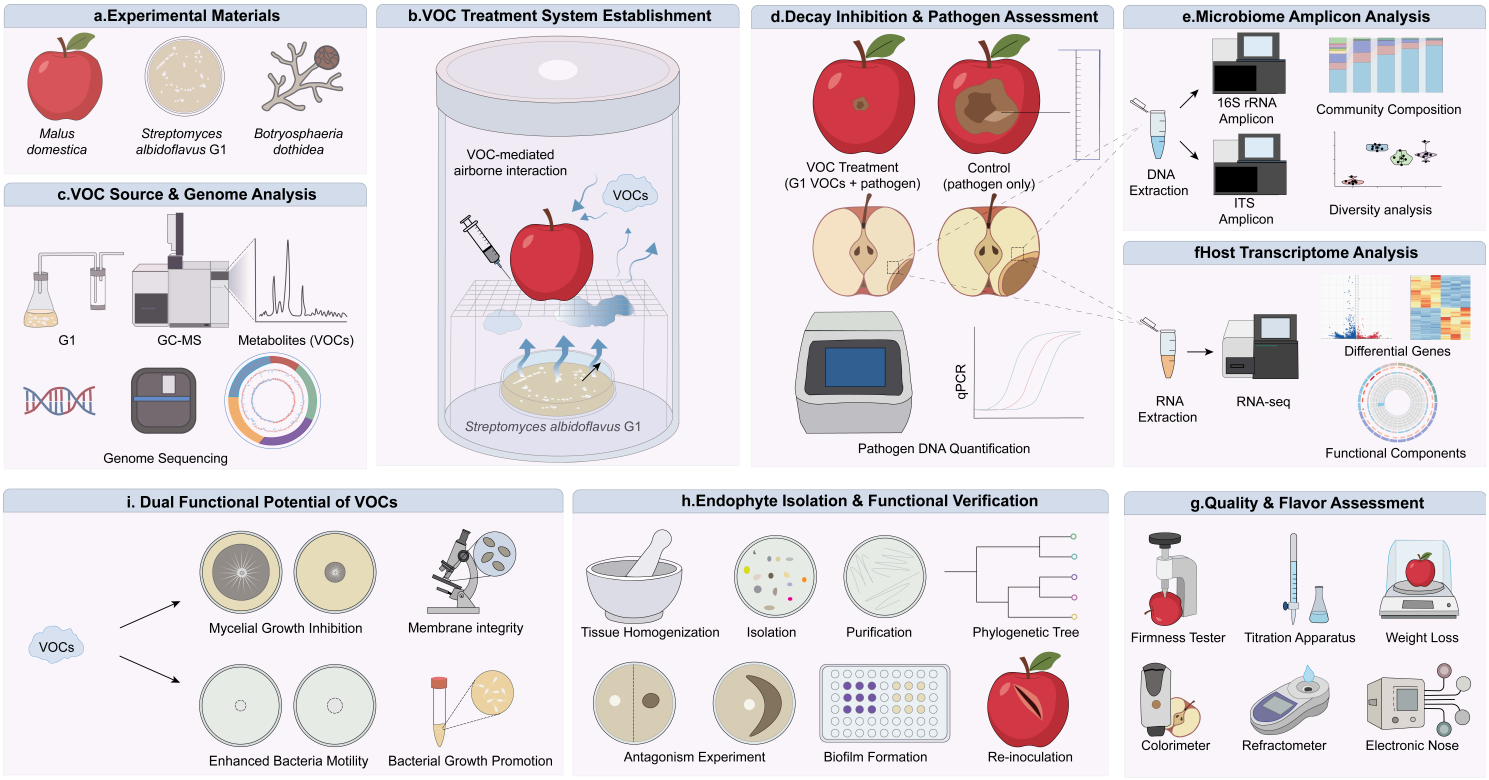


Figure 1

Experimental flow charts for this study. A) *Malus domestica* 'Red Fuji' cultivar was used in this study. *S. albidoflavus* and *B. dothidea* were isolated from asymptomatic and symptomatic apples respectively. B) G1-VOC mediated airborne interaction system was established. C) Volatilome profiling of G1-VOCs and whole genome sequencing of G1. D) lesion diameter *B. dothidea* abundance was quantified. E) apple microbiome was analysed by 16SrRNA and ITS amplicon sequencing. F) transcriptomic analysis to identify host differential gene expression G) apples were assessed for post-harvest quality indices. H) isolation and functional verification of endophytes, including antagonism and biofilm formation assays; and **(9)** characterization of the dual functional potential of G1-VOCs in inhibiting fungal growth while promoting beneficial bacterial motility and growth.

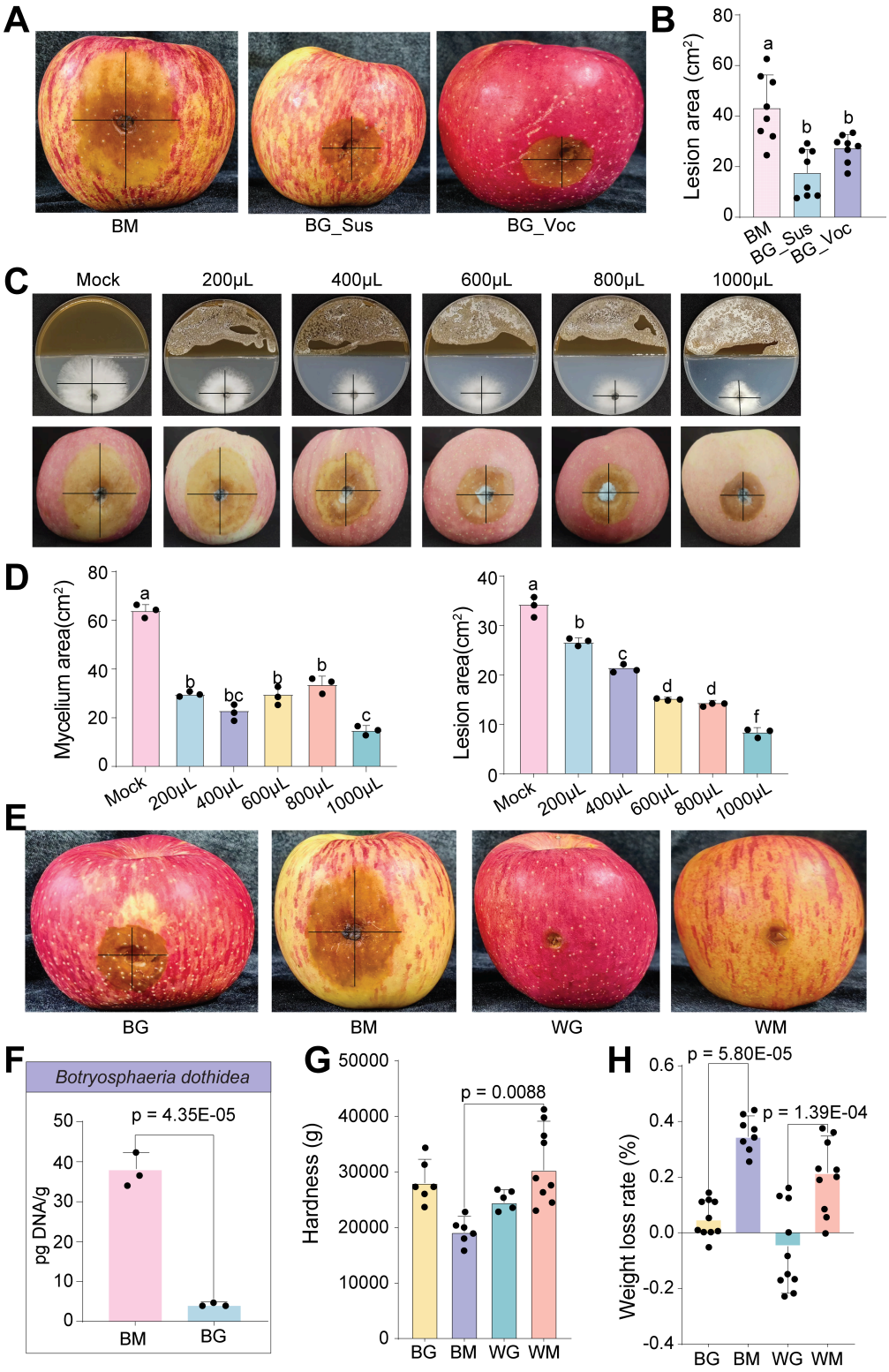


Figure 2

Biocontrol efficacy of *S. albidoflavus* G1-VOCs against *B. dothidea* and impact on apple quality. (A–B) Comparison of lesion areas in apples treated with mock (BM), G1 suspension (BG_Sus), and G1-VOCs (BG_Voc), showing significant disease suppression by both G1 treatments. **(C–D)** Dose-dependent inhibition of fungal mycelia and apple lesions by increasing volumes of G1-VOCs (200–1000 μL). **(E)** Visual representation across experimental groups (BG, BM, WG, WM). **(F)** *B. dothidea* DNA quantification

via qPCR, revealing a significant reduction in *B. dothidea* load within BG apples. **(G–H)** Assessment of fruit hardness and weight loss rate, indicating enhanced preservation of post-harvest quality in VOC-treated samples. Data represent mean ±SD; different letters or p-values indicate statistical significance.

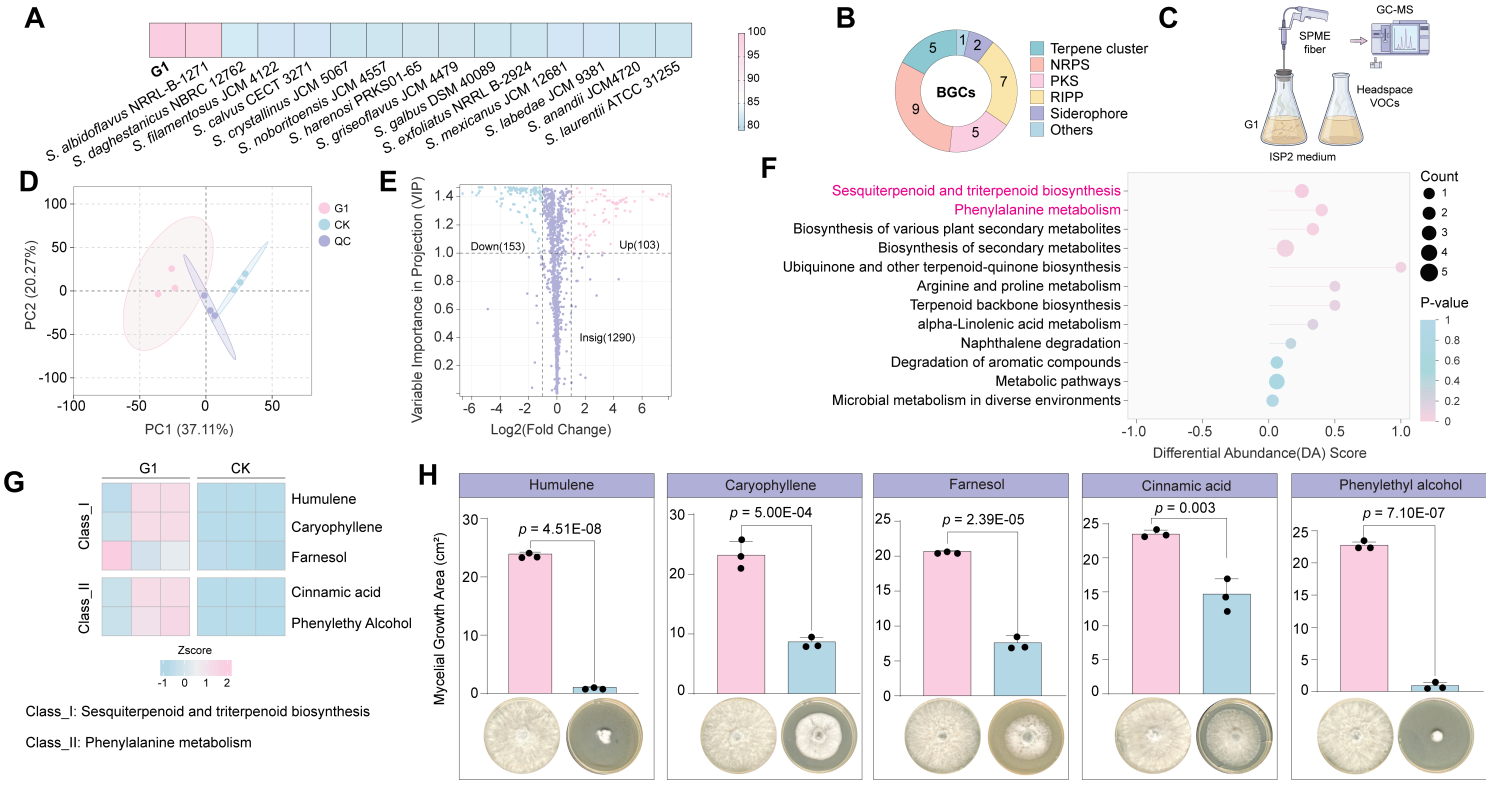


Figure 3

Genomic profiling, volatilome characterization, and antifungal validation of *Streptomyces albidoflavus*G1. (A)ANI heatmap confirming G1 taxonomic identity relative to other *Streptomyces*species. **(B)** Distribution of genomic biosynthetic gene clusters (BGCs) identified in the G1 genome, including terpenes **(C)** SPME-GC-MS experimental workflow. **(D)** PCA plot showing distinct metabolic clustering of G1 and CK. **(E)** Volcano plot of differential VOCs based on VIP and fold-change. **(F)** DA score plot highlighting enriched KEGG pathways with sesquiterpenoid, triterpenoid, and phenylalanine metabolism showing the highest enrichment. **(G)** Heatmap of upregulated VOCs from sesquiterpenoid, triterpenoid, and phenylalanine metabolism. **(H)** *In vitro* inhibition of *B. dothidea* by representative VOCs. Data are mean ± SD; p-values indicate significance via Student's t-test.

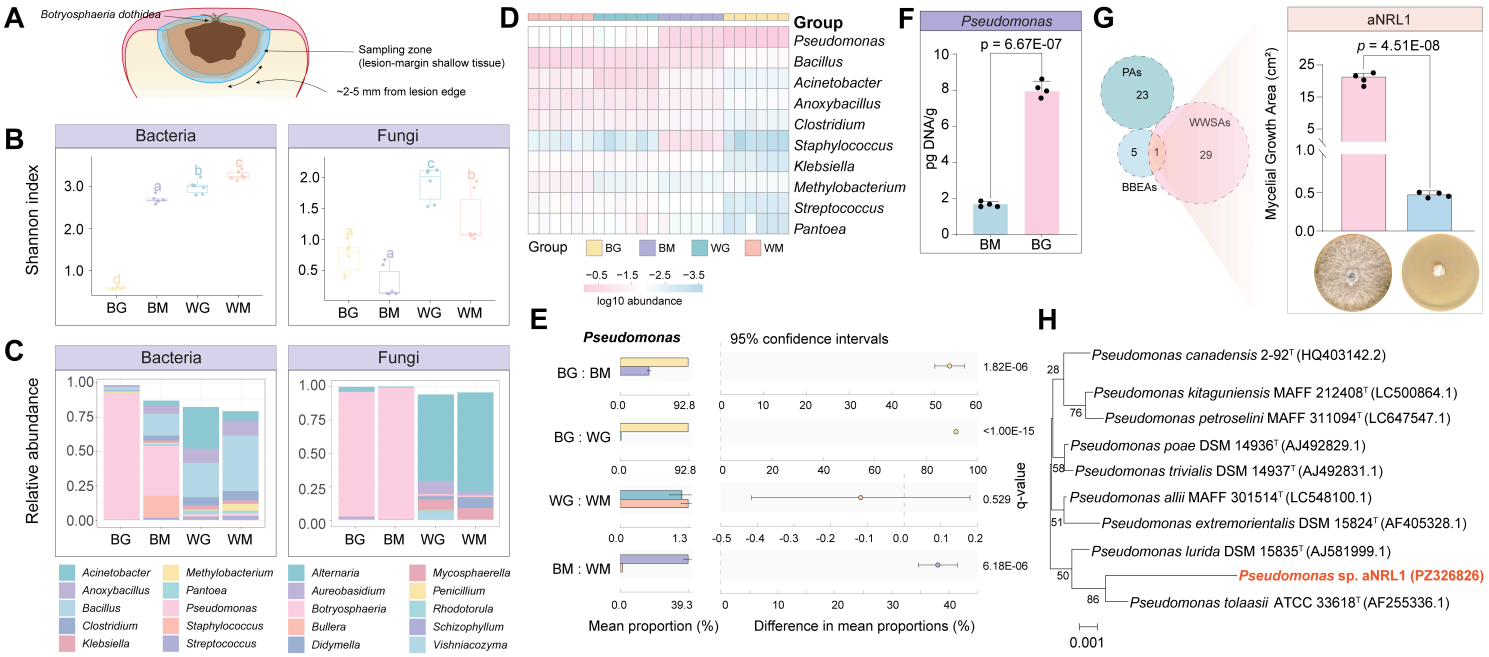


Figure 4

Impact of G1-derived VOCs on the apple fruit microbiome and recruitment of antagonistic *Pseudomonas*. (A) Schematic of the sampling zone at the lesion margin. **(B)** Alpha diversity (Shannon index) of bacterial and fungal communities across treatments. **(C)** Relative abundance of dominant bacterial and fungal genera. **(D)** Heatmap showing $\log_{10}$ abundance of key bacterial taxa, highlighting the enrichment of *Pseudomonas* in the BG group. **(E)** Extended error bar plots illustrating significant differences in *Pseudomonas* proportions between groups. **(F)** qPCR absolute quantification of *Pseudomonas* DNA in BM and BG groups. **(G)** Venn diagram of core taxa and *in vitro* growth inhibition of *B. dothidea* by the recruited isolate *Pseudomonas* sp. aNRL1. **(H)** Phylogenetic positioning of isolate aNRL1. Different letters in **B** indicate significant differences ($p < 0.05$); p-values in **F** and **G** indicate significance via Student's t-test.

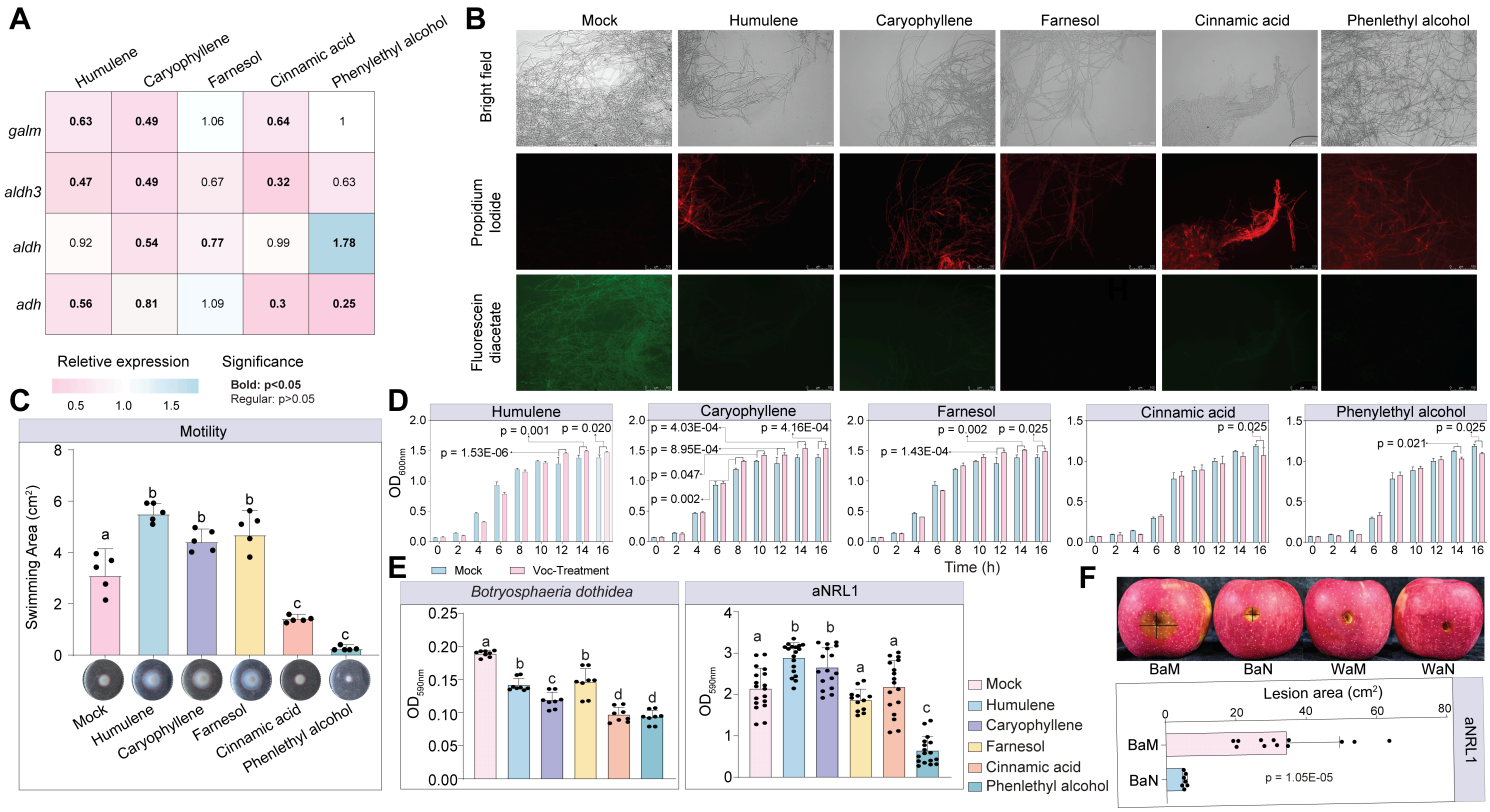


Figure 5

Mechanistic insights into the antimicrobial effects of G1-derived VOCs on *B. dothidea*and the recruited antagonist aNRL1. (A)Heatmap summarizing the relative expression of metabolic genes in *B. dothidea* under VOC exposure; bold values indicate statistical significance (). **(B)** Fluorescence microscopy of *B. dothidea* hyphae stained with Propidium Iodide (PI, red) and Fluorescein Diacetate (FDA, green), indicating membrane damage and loss of viability following VOCs treatment. **(C)**Motility assays of *Pseudomonas* sp. aNRL1, showing varied swimming area responses to different VOCs. **(D)** Growth kinetics of *Pseudomonas*sp. aNRL1 over 16 hours in the presence of specific VOCs. **(E)** Biofilm formation capacity of *B. dothidea* and aNRL1 under VOCs treatment. **(F)**Representative images and quantitative analysis of lesion areas on apple fruits, demonstrating the protective effect of aNRL1 against pathogen infection. Different letters and values indicate statistical significance via ANOVA or Student's t-test.

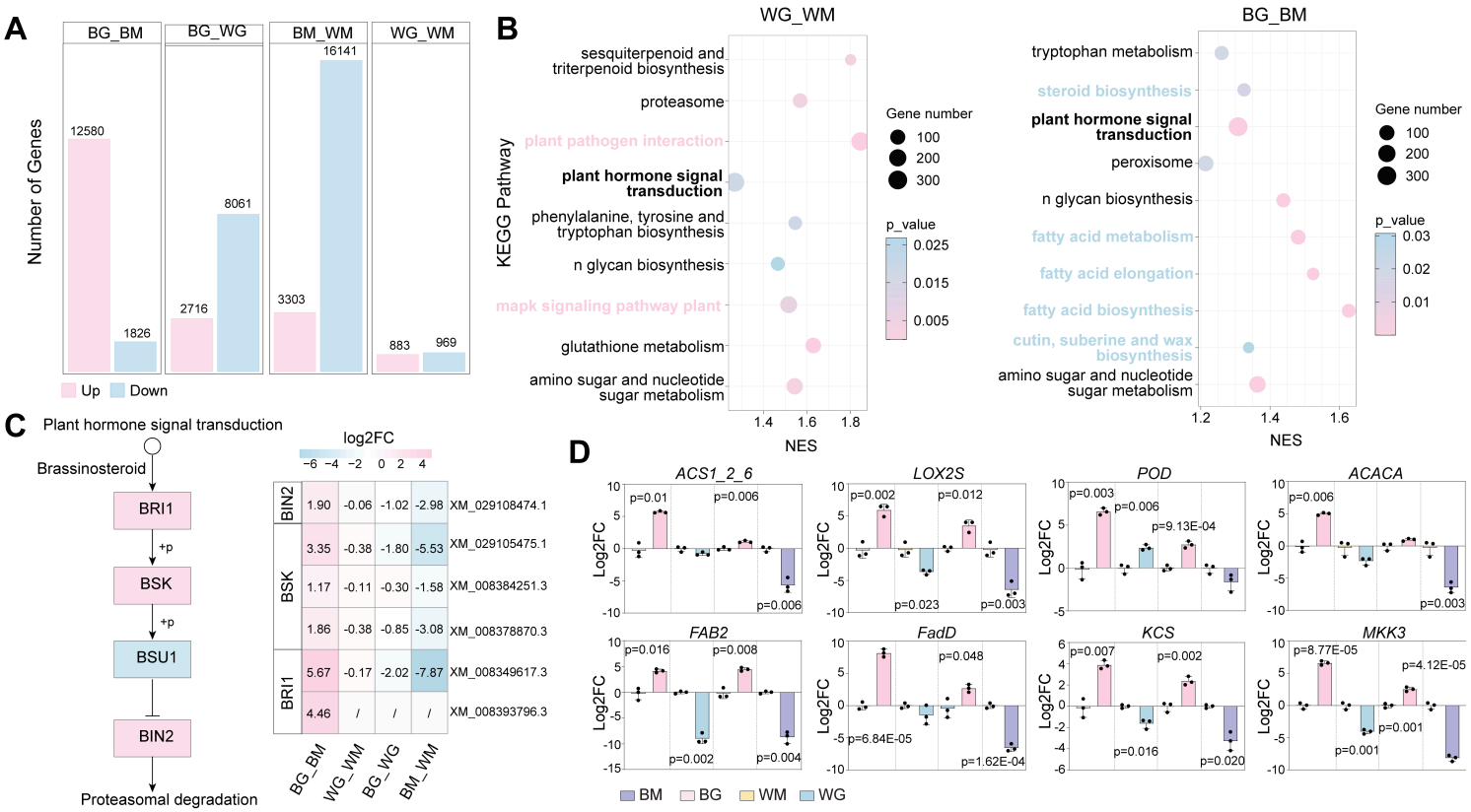


Figure 6

Transcriptional regulation and defense signaling in apple fruit during G1-VOC treatment and *B. dothidea*infection. A) Distribution of differentially expressed genes (DEGs) across treatments B) Dot plots of Gene Set Enrichment Analysis (GSEA) of KEGG pathways. The pink (WG_WM) denotes to pathways related to defense priming; blue (BG_BM) denotes to pathways related to stress response C) Brassinosteroid (BR) signaling: Heatmap of log_2FC values shows G1-VOCs reactivate the BR cascade (*BRI1*, *BSK*, *BIN2*) during infection, reversing pathogen-induced suppression D) RT-qPCR validation. Expression levels of eight key DEGs confirm RNA-Seq results. Data represent mean ± SD (n=3). Genes cover ethylene biosynthesis, antioxidant response, MAPK signaling, and wax/lipid synthesis.

Supplementary Files

This is a list of supplementary files associated with this preprint. Click to download.

- Supplementarytable.xlsx
- Supplementary.docx
- fig7.png